Large eddy simulation model for two-way coupled particle-laden turbulent flows

M. Hausmann, F. Evrard,* and B. van Wachem†
Chair of Mechanical Process Engineering, Otto-von-Guericke-Universität Magdeburg, Universitätsplatz 2, 39106 Magdeburg, Germany

(Received 20 February 2023; accepted 24 July 2023; published 11 August 2023)

In this paper, we propose a modeling framework for large eddy simulations of particle-laden turbulent flows that captures the interaction between the particle and fluid phase on both the resolved and subgrid scales. Unlike the vast majority of existing subgrid-scale models, the proposed framework not only accounts for the influence of the subgrid-scale velocity on the particle acceleration but also considers the effect of the particles on the turbulent fluid flow. This includes the turbulence modulation of the subgrid scales by the particles, which is taken into account by the modeled subgrid-scale stress tensor and the effect of the unresolved particle motion on the resolved flow scales. Our modeling framework combines a recently proposed model for enriching the resolved fluid velocity with a subgrid-scale component, with the solution of a transport equation for the subgrid-scale kinetic energy. We observe very good agreement of the particle pair separation and particle clustering compared to the corresponding direct numerical simulation. Furthermore, we show that the change of subgrid-scale kinetic energy induced by the particles can be captured by the proposed modeling framework.

DOI: 10.1103/PhysRevFluids.8.084301

I. INTRODUCTION

To capture particle-turbulence interactions within the whole turbulence spectrum down to the Kolmogorov length and timescale, a direct numerical simulation (DNS) has to be performed. For academic cases, DNSs of particle-laden turbulent flow is commonly used to gain insights into the underlying physical phenomena. As the flow configurations become more relevant for practical applications, however, resolving such a wide range of flow length and timescales becomes prohibitively expensive. An established surrogate in single phase flows is large eddy simulation (LES), which resolves only the large flow scales and models the mainly dissipative effect of the small scales. Even though many challenges still remain, LES is commonly applied to different single phase flow applications. Severe problems can arise, however, if particle-laden flows are considered, especially if the particles significantly affect the flow (two-way coupling).

The majority of the literature on particle-laden flows focuses on the one-way coupling, where the modification of the particle statistics by the flow is considered but not the effect of the particles on the flow. The effect of neglecting the subgrid-scale velocity contributions on the transport of the particles has been investigated and quantified in a variety of studies [1–4]. It has been observed that even though the kinetic energy of the subgrid-scale velocity is small, the consequence of neglecting

*Also at Sibley School of Mechanical and Aerospace Engineering, Cornell University, Ithaca, New York 14853, USA.
†berend.vanwachem@ovgu.de

the subgrid-scale fluid velocity on the motion of the particles can strongly affect the preferential concentration and other statistics of the particles.

There are several classes of models that attempt to produce realistic particle statistics in the scope of LES. Lagrangian models typically rely on the solution of a stochastic differential equation for every individual particle (see, e.g., Fede *et al.* [5], Bini and Jones [6], Berrouk *et al.* [7], Shotorban and Mashayek [8], Pozorski and Apte [9], and Knorps and Pozorski [10]). These models are typically simple to implement, computationally efficient, and can also be applied in complex domains. However, they usually contain empirical parameters and their Lagrangian nature prevents them from predicting accurate particle pair statistics. Other models rely on successive deconvolution of the LES velocity and use the resulting fluid velocity field to transport the particles [11,12]. Park *et al.* [13] extended the deconvolution of the filtered velocity by dynamically adjusting an elliptic differential filter such that the model is either kinetic energy or dissipation consistent with the subgrid-scale model. The main drawback of approximate deconvolution methods is that they do not introduce velocities with higher wave numbers than the LES, but only modify the LES velocity. That is why these models are not able to reproduce the particle statistics of a DNS to the full extent.

The most promising predictions of particle statistics using a LES framework are obtained with models that reconstruct the subgrid-scale velocity. Bassenne *et al.* [14] proposed such a model that alternatingly applies the dynamic approximate deconvolution of Park *et al.* and a spectral extrapolation based on the work of Domaradzki and Loh [15]. The proposed model improves the prediction of particle clustering for a wide range of Stokes numbers. However, the model requires a projection operation that has to be carried out with a resolution comparable to the DNS to obtain a divergence-free subgrid-scale velocity, which introduces prohibitively high computational costs. The kinematic simulation is a much cheaper approach and relies on the reconstruction of the subgrid-scale velocity using a truncated Fourier series [16–18]. The Fourier coefficients required for the kinematic simulation are chosen such that the resulting velocity field is divergence-free and matches a given kinetic energy spectrum. Even though kinematic simulations yield improved predictions of particle clustering for Stokes numbers $\mathrm{St} > 1.5$, it only applies to spatially homogeneous problems. Considering the available models, there still does not exist a model that yields satisfying improvements in predicting particle clustering and the Lagrangian particle statistics, while maintaining important features for practical applicability, such as a reasonable computational cost and the absence of empirical model parameters of critical influence.

Extensive research has been carried out to better understand the modulation of turbulence by particles. Studies of forced and decaying homogeneous isotropic turbulence (HIT) have shown that the presence of particles can modify the total dissipation in two ways [19–23]: (i) The particles can remove or add kinetic energy to the turbulent flow. The sign of the particle kinetic energy transfer and the scales at which the kinetic energy transfer occurs have been shown to depend on at least three parameters: the Stokes number, the particle number density, and the mass fraction [21]. (ii) The fluid dissipation is influenced by the presence of particles [19]. Similarly, depending on the characteristic turbulence and particle parameters and on the considered length scales, the fluid dissipation can either be enhanced or diminished.

A LES only resolves part of the kinetic energy spectrum and can thus only account directly for a modified total dissipation at the resolved scales. While the particle dissipation at the subgrid scale is fully disregarded in a classical LES, the subgrid-scale fluid dissipation is assumed to be equal to the fluid dissipation of a single phase flow. Classical LES uses one of the many subgrid-scale models designed for single phase flows (see, e.g., Sagaut [24]) and a fluid-particle coupling force obtained without information of the subgrid-scale fluid velocity at the particle positions. The application of several single-phase subgrid-scale models to particle-laden flows has been investigated by Boivin *et al.* [25], displaying very different results between the models. Boivin *et al.* also argued that at high particle mass fractions, the modeling error in predicting the fluid dissipation becomes less important, since the particle dissipation is then dominant. In fact, we show in the present paper that the neglected portion of the particle dissipation and fluid dissipation partially compensate each other. Rohilla *et al.* [26] showed that the Smagorinsky or dynamic Smagorinsky model applied to

particle-laden flows is unable to predict the critical particle volume loading at which the turbulence in a channel flow collapses (i.e., the flow becomes laminar). They state that one of the main reasons for this issue is the error made in modeling subgrid-scale dissipation.

Due to the complexity of two-way coupled turbulent particle-laden flows, models that account for all the coupling effects between the particles and all fluid length and timescales are very rare. An attempt has been made by Yuu *et al.* [27], who derived an algebraic model for the subgrid-scale kinetic energy that serves as input for a turbulent viscosity. In the studies of Pannala and Menon [28] and Sankaran and Menon [29], a source term accounting for the presence of particles is added to an evolution equation for the subgrid-scale kinetic energy equation, in a manner somewhat similar to the method presented in this paper. However, their particle source term is not closed because it contains the subgrid-scale velocity, which requires additional modeling.

In this paper, we present a framework that accounts for particle turbulence interactions that are typically neglected in a LES. The framework contains two coupled models: (i) a subgrid-scale model based on the localized dynamic kinetic energy model (LDKM) of Menon and coworkers [30,31], with an additional source term accounting for the influence of the particles on the subgrid-scale kinetic energy, and (ii) a model for the subgrid velocity that is used to close the particle equations of motion and the particle source terms in the momentum and subgrid-scale kinetic energy equations [32]. In Sec. II, the general numerical framework for treating the particle-laden flows in this paper is introduced, including the transport equation for the subgrid-scale kinetic energy upon which the subgrid-scale model is built. Section III gives an overview of the closures that are required in a particle-laden LES and provides a derivation of the proposed modeling framework. Subsequently, simulation setups for one-way and two-way coupled HIT are introduced in Sec. IV, and results of the comparison between DNS, LES, and modeled LES are presented in Sec. V. Finally, Sec. VI concludes the present paper.

II. GENERAL NUMERICAL FRAMEWORK

In this paper, we consider an incompressible fluid with density ρ_f and kinematic viscosity ν_f in the absence of a gravitational field. The fluid is laden with particles of index p having a density ρ_p and volume V_p. By volume filtering the Navier-Stokes equations (NSEs), the effect of the particles on the fluid can be modeled without needing to solve for the detail of the flow around each individual particle. The following equations are commonly used to approximate the volume-filtered velocity $\boldsymbol{u}$ and pressure p for small particle volume fractions (see, e.g., Maxey [33]):

$$\nabla \cdot \boldsymbol{u} = 0, \tag{1}$$

$$\frac{\partial \boldsymbol{u}}{\partial t} + \nabla \cdot (\boldsymbol{u} \otimes \boldsymbol{u}) = -\frac{1}{\rho_\mathrm{f}} \nabla p + \nabla \cdot \boldsymbol{\sigma} - \frac{1}{\rho_\mathrm{f}} \sum_p g(|\boldsymbol{x} - \boldsymbol{x}_p|) \boldsymbol{F}_p, \tag{2}$$

where $\boldsymbol{\sigma} = \nu_\mathrm{f}(\nabla \boldsymbol{u} + (\nabla \boldsymbol{u})^\mathrm{T})$ is the Newtonian viscous stress tensor and $\boldsymbol{F}_p$ is the sum of the fluid-particle interface forces of the particle with index p that can originate from drag, lift, added mass, or other effects. Gravity is neglected in the present paper. The kernel g of the volume filtering operation (see, e.g., Anderson and Jackson [34]) corresponds to filter size δ. Note that the filtering is only applied over volumes that are occupied by the fluid. Strictly speaking, the solution of Eqs. (1) and (2) is the approximation of volume-filtered quantities, which is not equivalent to the actual fluid velocity and pressure. In a simulation, the smallest resolvable flow structures are related to the smallest affordable cell size of the numerical grid. Similar to the LES approach, the volume-filtered approach solves for the large scales that can be resolved by the grid and models the effect of the small scales. It should be noted that in this paper, the influence of particle volume fraction α_p is not considered in the governing equations of the DNS and LES, even though it can be significant in dense particle regimes (i.e., $\alpha_\mathrm{p} > 0.01$). The proposed modeling is also only valid for dilute regimes.

Particles are considered as Lagrangian rigid point-particles. The particle position $\boldsymbol{x}_p$ is governed by the equation

$$\frac{d\boldsymbol{x}_p}{dt} = \boldsymbol{v}_p, \tag{3}$$

and the particle velocity by Newton's second law:

$$\frac{d\boldsymbol{v}_p}{dt} = \frac{1}{\rho_p V_p}\boldsymbol{F}_p. \tag{4}$$

There are a variety of mechanisms that lead to different forces acting on the particle, and additional source terms can arise in Eq. (4) if, e.g., gravity is considered, which is neglected in this paper. A summary of the possible force contributions and the regimes whereby their consideration is important has been provided by Kuerten [35].

We only consider cases in which the particles are significantly smaller than the Kolmogorov length scale (i.e., the smallest turbulent structures). The turbulence of the scales down to the Kolmogorov length scale are resolved with the DNS. Note that the DNS is based on the assumption of point particles. In cases, where not even the smallest flow structures can be resolved by the numerical grid, a LES can be performed. The governing equations for the LES are obtained by filtering Eqs. (1) and (2) once more with a filter G of width Δ, with $\Delta \gg \delta$:

$$\nabla \cdot \tilde{\boldsymbol{u}} = 0, \tag{5}$$

$$\frac{\partial \tilde{\boldsymbol{u}}}{\partial t} + \nabla \cdot \widetilde{(\boldsymbol{u} \otimes \boldsymbol{u})} = -\frac{1}{\rho_\mathrm{f}}\nabla \tilde{p} + \nabla \cdot \tilde{\boldsymbol{\sigma}} - \frac{1}{\rho_\mathrm{f}} \sum_p \widetilde{g(|\boldsymbol{x} - \boldsymbol{x}_p|)\boldsymbol{F}_p}. \tag{6}$$

Note that the filter G is applied to already continuous quantities (due to the previous filtering with g) and $\tilde{\cdot}$ represents the filtering operator. No further assumptions are introduced with the second filter level.

Due to the fact that the particles are much smaller than the Kolmogorov length scale (and therefore of the grid spacing), the numerical discretization of the source terms is realized with the particle-source-in-cell (PSIC) method of Crowe *et al.* [36],

$$\sum_p g(|\boldsymbol{x} - \boldsymbol{x}_p|)\boldsymbol{F}_p \approx \frac{1}{V_\mathrm{cell}(\boldsymbol{x})} \sum_{p \in \Omega_\mathrm{cell}(\boldsymbol{x})} \boldsymbol{F}_p \tag{7}$$

and

$$\sum_p \widetilde{g(|\boldsymbol{x} - \boldsymbol{x}_p|)\boldsymbol{F}_p} \approx \frac{1}{\tilde{V}_\mathrm{cell}(\boldsymbol{x})} \sum_{p \in \tilde{\Omega}_\mathrm{cell}(\boldsymbol{x})} \boldsymbol{F}_p, \tag{8}$$

where Ω_cell and $\tilde{\Omega}_\mathrm{cell}$ indicate computational cells of the DNS and the LES, respectively, and $V_\mathrm{cell} < \tilde{V}_\mathrm{cell}$ their volumes.

For the modeling of the flow scales that are filtered out by kernel G, a transport equation for the subgrid-scale kinetic energy $K_\mathrm{sgs} = 1/2(\widetilde{\boldsymbol{u} \cdot \boldsymbol{u}} - \tilde{\boldsymbol{u}} \cdot \tilde{\boldsymbol{u}})$ is derived. This is done in two steps. First, Eq. (2) is dotted with the velocity $\boldsymbol{u}$ and subsequently filtered with G, which yields

$$\begin{aligned}\frac{1}{2}\frac{\partial \widetilde{\boldsymbol{u} \cdot \boldsymbol{u}}}{\partial t} + \frac{1}{2}\nabla \cdot \widetilde{(\boldsymbol{u} \otimes \boldsymbol{u} \cdot \boldsymbol{u})} \\ = -\frac{1}{\rho_\mathrm{f}}\nabla \cdot \widetilde{(p\boldsymbol{u})} + \nabla \widetilde{(\boldsymbol{\sigma} \cdot \boldsymbol{u})} - \widetilde{\nabla \boldsymbol{u} : \boldsymbol{\sigma}} - \frac{1}{\rho_\mathrm{f} \tilde{V}_\mathrm{cell}} \sum_{p \in \tilde{\Omega}_\mathrm{cell}} \boldsymbol{F}_p(\boldsymbol{u}(\boldsymbol{x}_p)) \cdot \boldsymbol{u}(\boldsymbol{x}_p).\end{aligned} \tag{9}$$

The last term on the right-hand side is realized by multiplying the fluid-particle interface forces $\boldsymbol{F}_p$ with the fluid velocity at the particle position and taking the sum over all particles within a LES grid cell. In the following, we will emphasize that the forces $\boldsymbol{F}_p$ require the unfiltered fluid velocity

at the particle position by explicitly writing its dependency on $\boldsymbol{u}(\boldsymbol{x}_p)$. The reader may be reminded, however, that the forces may also depend on additional parameters.

The sum over all particles within a LES grid cell replaces the filtering operation $\widetilde{\boldsymbol{F}_p \cdot \boldsymbol{u}}$. In fact, this resembles the approach of Schumann [37], who defines a set of LES equations based on averaging over the volume of the computational cell, which is arguably closer to the numerical realization of a LES than a spatially continuous filtering operation. Second, Eq. (6) is dotted with the filtered velocity $\tilde{\boldsymbol{u}}$, which leads to

$$\begin{aligned}&\frac{1}{2}\frac{\partial \tilde{\boldsymbol{u}}\cdot\tilde{\boldsymbol{u}}}{\partial t}+\frac{1}{2}\nabla\cdot(\widetilde{\boldsymbol{u}\otimes\boldsymbol{u}}\cdot\tilde{\boldsymbol{u}})\\&\quad=-\frac{1}{\rho_\mathrm{f}}\nabla\cdot(\widetilde{p\tilde{\boldsymbol{u}}})+\nabla\cdot(\widetilde{\boldsymbol{\sigma}}\cdot\tilde{\boldsymbol{u}})-\nabla\tilde{\boldsymbol{u}}:\widetilde{\boldsymbol{\sigma}}-\frac{1}{\rho_\mathrm{f}\tilde{V}_\mathrm{cell}}\tilde{\boldsymbol{u}}\cdot\sum_{p\in\tilde{\Omega}_\mathrm{cell}}\boldsymbol{F}_p(\boldsymbol{u}(\boldsymbol{x}_p)).\end{aligned}\tag{10}$$

The numerical realization of the last term on the right-hand side includes a sum of the forces $\boldsymbol{F}_p$ within a LES grid cell and subsequent multiplication with the LES velocity of the present grid cell.

Subtracting Eq. (10) from Eq, (9) yields an equation for K_sgs:

$$\begin{aligned}&\frac{\partial K_\mathrm{sgs}}{\partial t}+\frac{1}{2}\frac{\partial}{\partial x_j}(\widetilde{u_iu_ju_i}-\widetilde{u_iu_j}\tilde{u}_i)\\&\quad=-\frac{1}{\rho_\mathrm{f}}\frac{\partial}{\partial x_i}(\widetilde{pu_i}-\tilde{p}\tilde{u}_i)+\nu_\mathrm{f}\frac{\partial^2 K_\mathrm{sgs}}{\partial x_j\partial x_j}-\nu_\mathrm{f}\left(\widetilde{\frac{\partial u_i}{\partial x_j}\frac{\partial u_i}{\partial x_j}}-\frac{\partial\tilde{u}_i}{\partial x_j}\frac{\partial\tilde{u}_i}{\partial x_j}\right)\\&\qquad-\frac{1}{\rho_\mathrm{f}\tilde{V}_\mathrm{cell}}\left(\sum_{p\in\tilde{\Omega}_\mathrm{cell}}F_{i,p}(\boldsymbol{u}(\boldsymbol{x}_p))u_i(\boldsymbol{x}_p)-\tilde{u}_i\sum_{p\in\tilde{\Omega}_\mathrm{cell}}F_{i,p}(\boldsymbol{u}(\boldsymbol{x}_p))\right).\end{aligned}\tag{11}$$

The last term on the right-hand side is the source term due to the subgrid-scale kinetic energy transfer by the particles. This equation is the foundation for the modeling of the turbulence modulation by particles of scales that are filtered out by G.

III. MODELING IN THE LES FRAMEWORK

The second filtering operation with G leads to equations governing the fluid behavior that cannot be solved explicitly without knowing the fluid velocity $\boldsymbol{u}$. We model these equations in the framework of a LES. In addition to the modeling of the subgrid-scale stress tensor, a particle-laden flow requires further closures, which are first explained and then modeled.

A. Required closures

The fluid equations with the assumption of a dilute particle-laden flow with sufficiently small particles and subsequent filtering with the kernel G can be written in the typical form of a LES [38] as

$$\frac{\partial\tilde{u}_i}{\partial x_i}=0,\tag{12}$$

$$\frac{\partial\tilde{u}_i}{\partial t}+\tilde{u}_j\frac{\partial\tilde{u}_i}{\partial x_j}=-\frac{1}{\rho_\mathrm{f}}\frac{\partial\tilde{p}}{\partial x_i}+\nu_\mathrm{f}\frac{\partial^2\tilde{u}_i}{\partial x_j\partial x_j}-\frac{\partial\tau_{ij}}{\partial x_j}-\frac{1}{\rho_\mathrm{f}\tilde{V}_\mathrm{cell}}\sum_{p\in\tilde{\Omega}_\mathrm{cell}}F_{\mathrm{D},i,p}(\boldsymbol{u}(\boldsymbol{x}_p)),\tag{13}$$

where we assumed that only the drag force $\boldsymbol{F}_D$ acts on the particles. The subgrid-scale stress tensor τ_{ij} is defined as

$$\tau_{ij}=\widetilde{u_iu_j}-\tilde{u}_i\tilde{u}_j.\tag{14}$$

With the particle force reducing to the drag force, the particle velocity $\boldsymbol{v}_p$ is governed by

$$\frac{d\boldsymbol{v}_p}{dt} = \frac{1}{\rho_p V_p}\boldsymbol{F}_{\mathrm{D},p}(\boldsymbol{u}(\boldsymbol{x}_p)). \tag{15}$$

To solve for the filtered fluid velocity $\tilde{\boldsymbol{u}}$ and the particle velocity $\boldsymbol{v}_p$, two further modeling steps are required: (i) The subgrid-scale stress tensor τ_{ij} has to be closed to model the effect of the unresolved subgrid scales on the resolved (filtered) quantities. It should be noted that the presence of the particles modifies the subgrid-scale velocity. As a consequence, models for the subgrid-scale stress tensor that are based on assumptions of the single-phase flow subgrid-scale velocity are, strictly speaking, not valid. (ii) To compute the drag force acting on the particle and vice versa, the force that is coupled back to the fluid with opposite sign, the unfiltered fluid velocity at the particle position is required, which is an unknown quantity in a LES. It is well understood that the particles behave differently when the drag force is obtained from the filtered fluid velocity at the particle position $\boldsymbol{F}_{\mathrm{D},p}(\tilde{\boldsymbol{u}}(\boldsymbol{x}_p))$ [2,3]. In the present paper, a modeling framework for both closures is provided.

B. Modeling the subgrid-scale stress tensor

The subgrid-scale stress tensor accounts for the effect of the subgrid-scale velocities on the velocity that is resolved in a LES. In a LES, this subgrid-scale stress tensor is modeled. Typically, the focus lies exclusively on modeling the energetic effects of the subgrid scales on the resolved scales, even though the mechanisms of turbulent energy transfer (vorticity stretching and strain self-amplification) possess characteristic directional dependencies [39]. In single phase turbulent flows, the construction of the subgrid-scale model can be based on the assumption that the energy transferred towards smaller scales is either dissipated by the viscosity or scattered back towards larger scales. In a particle-laden turbulent flow, however, additional energy sources and sinks occur due to the interactions with the particles that classical subgrid-scale models (designed for single phase flows) do not account for.

To take the interactions of the fluid with the particles into account, we modify the LDKM of Menon and coworkers [30,31]. The modeling of the subgrid-scale stress tensor is based on an eddy viscosity ν_k,

$$\tau_{ij} = -2\nu_\mathrm{k}\tilde{S}_{ij} + \tfrac{2}{3}K_\mathrm{sgs}\delta_{ij}, \tag{16}$$

where $\tilde{S}_{ij}$ is the filtered strain-rate tensor and δ_{ij} is the Kronecker tensor. The eddy viscosity is computed from the subgrid-scale kinetic energy,

$$\nu_\mathrm{k} = C_\mathrm{k}\sqrt{K_\mathrm{sgs}}\Delta, \tag{17}$$

where C_k is a constant. The evolution of the subgrid-scale kinetic energy K_sgs is governed by the transport Eq. (11). However, several terms of the transport equation for K_sgs require the unfiltered fluid velocity. Lilly [40] introduced a model for the transport Eq. (11) (without particle source term), such that it can be solved by knowing filtered quantities only, which is the basis of the LDKM,

$$\frac{\partial K_\mathrm{sgs}}{\partial t} + \tilde{u}_i\frac{\partial K_\mathrm{sgs}}{\partial x_i} = -\tau_{ij}\frac{\partial \tilde{u}_i}{\partial x_j} - C_\epsilon\frac{K_\mathrm{sgs}^{3/2}}{\Delta} + \frac{\partial}{\partial x_i}\left(\nu_\mathrm{k}\frac{\partial K_\mathrm{sgs}}{\partial x_i}\right) + \Phi_\mathrm{P}, \tag{18}$$

where C_ϵ is a constant. The particle source term Φ_P is not part of the original LDKM but introduced in the present model based on the derivations in Sec II:

$$\Phi_\mathrm{P} = -\frac{1}{\rho_\mathrm{f}\tilde{V}_\mathrm{cell}}\left(\sum_{p\in\tilde{\Omega}_\mathrm{cell}} F_{\mathrm{D},i,p}(\boldsymbol{u}(\boldsymbol{x}_p))u_i(\boldsymbol{x}_p) - \tilde{u}_i\sum_{p\in\tilde{\Omega}_\mathrm{cell}} F_{\mathrm{D},i,p}(\boldsymbol{u}(\boldsymbol{x}_p))\right). \tag{19}$$

The particle source term represents the kinetic energy added to or removed from the subgrid-scale velocity by the particles. Although the source term is written as a function of the drag force, the

derivation in Sec. II shows that the source term can be computed from all the fluid-particle interface forces used in the fluid momentum equation, such as lift force or added mass force.

Note that Pannala and Menon [28] and Sankaran and Menon [29] already applied the concept of a particle source term in the transport equation of the subgrid-scale kinetic energy, but with a different realization and without providing a rigorous derivation. To distinguish the present model including the particle source term Eq. (19) from the original LDKM, we refer to it as modified LDKM (mLDKM). The constants C_ϵ and C_k are computed dynamically based on the assumption of scale similarity. The Leonard stress tensor is defined as

$$L_{ij} = \widehat{\tilde{u}_i \tilde{u}_j} - \hat{\tilde{u}}_i \hat{\tilde{u}}_j, \tag{20}$$

where $\hat{}$ indicates a filtering operation with the filter width $\hat{\Delta} = 2\Delta$. Assuming that the Leonard stress tensor is analogously computed to the subgrid-scale stress tensor,

$$L_{ij} = -2C_\mathrm{k}\hat{\Delta}K_\mathrm{test}^{1/2}\hat{\tilde{S}}_{ij} + \tfrac{1}{3}\delta_{ij}L_{kk}, \tag{21}$$

the constant C_k can be dynamically computed from

$$C_\mathrm{k} = \frac{1}{2}\frac{L_{ij}\sigma_{ij}}{\sigma_{lm}\sigma_{lm}}, \tag{22}$$

with

$$\sigma_{ij} = -\hat{\Delta}K_\mathrm{test}^{1/2}\hat{\tilde{S}}_{ij} \tag{23}$$

and

$$K_\mathrm{test} = \tfrac{1}{2}(\widehat{\tilde{u}_i\tilde{u}_i} - \hat{\tilde{u}}_i\hat{\tilde{u}}_i) = \tfrac{1}{2}L_{ii}. \tag{24}$$

Note that $\delta_{ij}\tilde{S}_{ij} = 0$ for incompressible flows.

Assuming the scale similarity to also be valid for the dissipation gives

$$C_\epsilon\frac{K_\mathrm{test}^{3/2}}{\hat{\Delta}} = (\nu_\mathrm{f} + \nu_\mathrm{k})\left(\widehat{\frac{\partial\tilde{u}_i}{\partial x_j}\frac{\partial\tilde{u}_i}{\partial x_j}} - \frac{\partial\hat{\tilde{u}}_i}{\partial x_j}\frac{\partial\hat{\tilde{u}}_i}{\partial x_j}\right). \tag{25}$$

With this, the dynamic value of C_ϵ can be obtained from

$$C_\epsilon = \frac{\hat{\Delta}(\nu_\mathrm{f} + \nu_\mathrm{k})}{K_\mathrm{test}^{3/2}}\left(\widehat{\frac{\partial\tilde{u}_i}{\partial x_j}\frac{\partial\tilde{u}_i}{\partial x_j}} - \frac{\partial\hat{\tilde{u}}_i}{\partial x_j}\frac{\partial\hat{\tilde{u}}_i}{\partial x_j}\right). \tag{26}$$

The original LDKM for single phase flows (without the particle source term) has some advantageous properties. The dynamical constant C_k can become negative and, thus, theoretically enables emulating the backward energy cascade. However, similar to Kim *et al.* [41], the eddy viscosity is numerically limited to $\nu_\mathrm{k} > -\nu_\mathrm{f}$ to ensure a stable numerical solution of the flow equations. In contrast to the dynamic model of Germano *et al.* [42], no averaging along statistically homogeneous directions is required with the LDKM, which requires the existence of statistically homogeneous directions. With the dynamic computation of the constants, the model does not contain any adjustable constants.

Besides the theoretical advantages of the LDKM in a single phase flow, the main advantage is that it provides a framework for incorporating the particle source term in a deterministic way. If the particles remove kinetic energy from the subgrid scales, K_sgs decreases and the fluid dissipation (i.e., the eddy viscosity) is reduced. However, the model is not capable of considering at which scales the enhancement or attenuation of turbulence takes place. In reality, the spectral distribution of the subgrid-scale kinetic energy can play an important role.

The particle source term Φ_P is not closed in the scope of LES because the unfiltered velocity at the particle position is required, whereas only the filtered velocity is available. Thus, the mLDKM

including the particle source term is only applicable if a suitable model for the subgrid-scale velocity at the particle position is provided.

C. Approximate reconstruction of the subgrid-scale velocity

The computation of the drag force acting on the particle requires knowledge of the fluid velocity at the particle positions, which is used in the equations of motion of the particles and as the feedback force on the fluid. In addition to the LES velocity, the subgrid-scale velocity has to be provided. We approximate the subgrid-scale velocity as a truncated Fourier-series expansion,

$$\boldsymbol{u}' = \sum_{m=0}^{N_\mathrm{m}-1} (\boldsymbol{A}_m(t)\cos(\boldsymbol{k}_m \cdot \boldsymbol{x}) + \boldsymbol{B}_m(t)\sin(\boldsymbol{k}_m \cdot \boldsymbol{x})), \tag{27}$$

where $\boldsymbol{A}_m(t)$ and $\boldsymbol{B}_m(t)$ are time-dependent coefficients, N_m the number of modes, and $\boldsymbol{k}_m$ the wave vectors. With similar coefficients for the entire domain, the subgrid-scale velocity is statistically homogeneous. To overcome the limitation of global statistical homogeneity, statistically homogeneous subdomains $\Omega_\mathrm{domain} \in \Omega$ are defined that own a distinct set of coefficients $\boldsymbol{A}_m(t)$ and $\boldsymbol{B}_m(t)$, respectively. Quantities that are known in the LES may be averaged over the subdomain,

$$\langle\phi\rangle_\mathrm{domain} = \frac{1}{V_\mathrm{domain}} \int_{\Omega_\mathrm{domain}} \phi dV, \tag{28}$$

where V_domain indicates the volume of a subdomain. We exploit the findings of Laval *et al.* [43] that suggest that the effects of the nonlinear term in the governing equations for the subgrid-scale velocity on the kinetic energy spectrum and intermittency may be replaced by an additional viscosity that can be obtained from renormalization groups [44],

$$\nu_\mathrm{t}'(k) = \left(\nu_\mathrm{f}^2 + C_\nu \int_k^\infty q^{-2} E(q) dq\right)^{1/2} - \nu_\mathrm{f}, \tag{29}$$

with the fluid kinetic energy spectrum E and an analytical constant $C_\nu = 2/5$. An equation to obtain a preliminary set of coefficients $A^*_{m,i}$ and $B^*_{m,i}$ can be derived [32]:

$$\begin{aligned}
&\frac{A^*_{m,i} - A^n_{m,i}}{\Delta t} + \langle\tilde{u}^n_j\rangle_\mathrm{domain}\left(k_{m,j} B^n_{m,i} + \frac{\partial A^n_{m,i}}{\partial x_j}\right) + A^n_{m,j}\left\langle\frac{\partial \tilde{u}^n_i}{\partial x_j}\right\rangle_\mathrm{domain} \\
&\quad = (\nu_\mathrm{f} + \nu_\mathrm{t}')\left(-|\boldsymbol{k}_m|^2 A^n_{m,i} + \frac{\partial^2 A^n_{m,i}}{\partial x_j \partial x_j} + 2k_{m,j}\frac{\partial B^n_{m,i}}{\partial x_j}\right) + f_{m,i},
\end{aligned} \tag{30}$$

$$\begin{aligned}
&\frac{B^*_{m,i} - B^n_{m,i}}{\Delta t} + \langle\tilde{u}^n_j\rangle_\mathrm{domain}\left(\frac{\partial B^n_{m,i}}{\partial x_j} - k_{m,j} A^n_{m,i}\right) + B^n_{m,j}\left\langle\frac{\partial \tilde{u}^n_i}{\partial x_j}\right\rangle_\mathrm{domain} \\
&\quad = (\nu_\mathrm{f} + \nu_\mathrm{t}')\left(-|\boldsymbol{k}_m|^2 B^n_{m,i} + \frac{\partial^2 B^n_{m,i}}{\partial x_j \partial x_j} - 2k_{m,j}\frac{\partial A^n_{m,i}}{\partial x_j}\right) + g_{m,i}.
\end{aligned} \tag{31}$$

Note that no summation over the index m is carried out. The index n indicates the time level and $f_{m,i}$ and $g_{m,i}$ are forcing terms to maintain a desired kinetic energy of the subgrid scales. The coefficients are made divergence-free by applying a subsequent projection operation to the preliminary coefficients

$$\boldsymbol{A}^{n+1}_m(t) = \boldsymbol{A}^*_m(t) - \boldsymbol{k}_m \frac{\boldsymbol{k}_m \cdot \boldsymbol{A}^*_m(t)}{|\boldsymbol{k}_m|^2}, \tag{32}$$

$$\boldsymbol{B}^{n+1}_m(t) = \boldsymbol{B}^*_m(t) - \boldsymbol{k}_m \frac{\boldsymbol{k}_m \cdot \boldsymbol{B}^*_m(t)}{|\boldsymbol{k}_m|^2}. \tag{33}$$

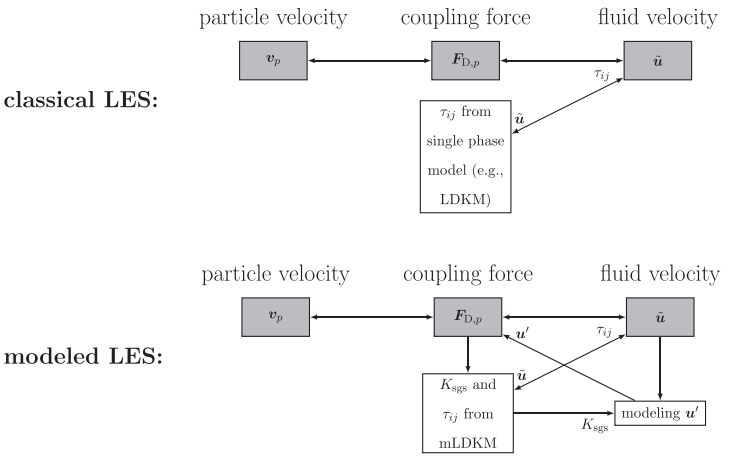

FIG. 1. Visualization of the modeled interactions in a classical LES (top) compared to the modeled interactions in the modeled LES (bottom).

Since with discretized spatial derivatives the solution for the coefficients essentially consists of explicit algebraic operations, the numerical solution is rather inexpensive. Numerical experiments show that the solution for the coefficients $A_{m,i}$ and $B_{m,i}$ requires a computing time of the same order as the LES [32].

The fact that every subdomain possesses a distinct set of coefficients requires the interpolation of the coefficients between the subdomains. In Hausmann *et al.* [32], an interpolation of the coefficients is presented that leads to a divergence-free subgrid-scale velocity field between subdomains. Homogeneous Dirichlet boundary conditions for the subgrid-scale velocity, as they occur in wall-bounded flows, may be realized by using the divergence free interpolation between the subdomains and the fluid velocity at the wall.

D. Coupling between the fluid phase and the particle phase

In a particle-laden LES, at least three effects are not or insufficiently considered: (i) The particles are accelerated by a drag force which requires the fluid velocity at the particle position. Using the filtered fluid velocity instead leads to different clustering and Lagrangian statistics of the particles [2,3]. (ii) The effect of the particles on the scales that are resolved in a LES is incomplete, since the feedback force is only computed from the filtered velocity instead of the unfiltered velocity. (iii) The effect of the particles on the subgrid scales is not considered in a classical LES. The modified subgrid-scale velocity changes the subgrid-scale stress tensor compared to a single phase flow (i.e., the dissipation by the subgrid-scale fluid velocity).

In Fig. 1, the procedure of a classical LES is compared to our proposed modeling framework that combines the mLDKM and the model for the subgrid-scale velocity. We refer to the latter as modeled LES. In the classical LES, the filtered fluid velocity $\tilde{\boldsymbol{u}}$ is obtained by solving the filtered NSE with a subgrid-scale stress tensor that is predicted by one of the subgrid-scale models commonly used for single phase flows. Note that subgrid-scale models for single phase flows do not incorporate information of the fluid-particle coupling force. The coupling force is computed from the filtered velocity at the particle position and is used to obtain the particle acceleration and the source terms in the fluid momentum equation.

The modeled LES exhibits a stronger coupling between the fluid phase and the particle phase. Using the filtered fluid velocity and the coupling force as input, the mLDKM returns a prediction of the subgrid-scale stress tensor, which is used for solving the filtered NSE and the subgrid-scale kinetic energy, which serves as the target kinetic energy for the generated subgrid-scale velocity.

With the modeled subgrid-scale velocity, the coupling force is computed considering all turbulent length and timescales down to the Kolmogorov scales. This enables a more realistic prediction of the particle velocity, the momentum source term in the filtered NSE, and the kinetic energy source term in the mLDKM. As a consequence, the subgrid-scale stress tensor and the modeled subgrid-scale velocity contain information about the turbulence modification by the particles at the unresolved scales. In theory, the modeled LES covers all occurring interactions between the fluid and the particles.

In Sec. V A, we also study one-way coupling simulations with the modeled LES, in which case all arrows of Fig. 1 that point from the coupling force to anything else than the particle velocity vanish. The mLDKM then reduces to the original LDKM or can be replaced by any subgrid-scale model that is developed for single phase flows. The subgrid-scale kinetic energy that is required as input for the modeling of the subgrid-scale velocity can be alternatively estimated with the model of Yoshizawa [45] or the dynamic model of Moin *et al.* [46].

IV. SIMULATIONS

Our proposed modeling is verified and validated by means of DNS and LES of particle-laden turbulent flows. For all the simulation cases, HIT is considered. First, the model for the subgrid-scale velocity at the particle position is assessed by comparing the particle statistics in the modeled LES with the particle statistics in a DNS of the same one-way coupled case of statistically stationary turbulence. In a second case, the feedback force of the particles on the fluid is investigated. This requires the full modeling framework as described in Sec. III D, which is evaluated by comparing the modeled LES and DNS of two-way coupled particle laden decaying turbulence. The subsequent sections provide details of the realizations and configurations of the simulations.

A. Solving the governing equations

The NSE are solved with a finite volume approach that is second order in space and time [47]. The continuity equation and the momentum equations are coupled using momentum weighted interpolation [48]. Therefore, two distinct velocity fields exist numerically, a cell-centered velocity accurately satisfying the momentum balance and a face centered velocity conserving mass.

Statistically steady turbulence is maintained by supplying the flow with energy through source terms in the momentum equations [49]. An important property of the forcing is that the artificial source terms can be introduced in a limited range of wave numbers, $k \in [k_{\text{start}}, k_{\text{end}}]$. For particle-laden flows, this is essential to avoid directly impacting the particle behavior by the forcing.

The particle equations of motion Eqs. (3) and (4) are solved with the Verlet scheme [50]. The drag force acting on the Lagrangian particle p is computed from

$$\boldsymbol{F}_{\mathrm{D},p} = C_{\mathrm{D}} \frac{\rho_{\mathrm{f}}}{8} \pi d_p^2 |\boldsymbol{u}_{\mathrm{rel}}| \boldsymbol{u}_{\mathrm{rel}}, \tag{34}$$

with the drag coefficient from the Schiller-Naumann correlation [51]

$$C_{\mathrm{D}} = \frac{24}{\mathrm{Re}_p} \left(1 + 0.15 \mathrm{Re}_p^{0.687}\right), \tag{35}$$

and the particle Reynolds number $\mathrm{Re}_p = |\boldsymbol{u}_{\mathrm{rel}}| d_p / \nu_{\mathrm{f}}$. The relative velocity $\boldsymbol{u}_{\mathrm{rel}}$ is defined as the difference between the fluid velocity at the particle position and the particle velocity $\boldsymbol{u}_{\mathrm{rel}} = \boldsymbol{u}(\boldsymbol{x}_p) - \boldsymbol{v}$.

To obtain the fluid velocity at the particle position, an interpolation from the Cartesian grid is required. An essential property of the interpolation scheme is that the interpolated velocity needs to be divergence-free. In the present paper, a second-order divergence-free interpolation from the face-centered velocity (that fulfills the continuity equation with high accuracy) to the particle position is applied [52].

TABLE I. Single phase flow parameters of the HIT simulation configuration.

Parameters	Values
Re_λ	75
Re_l	205
η/L	0.0017
$\tau_\eta/T_{\mathrm{ref}}$	0.0075
λ/L	0.029
l_{11}/L	0.079
$k_{\mathrm{start}}L/2\pi$	3
$k_{\mathrm{end}}L/2\pi$	6

In the case of the two-way coupling simulations, the PSIC method of Crowe *et al.* [36] is utilized.

B. Simulation setups

1. Single phase flow setups

The studies in this paper consist of two different flow types: (i) one-way coupling simulations of forced HIT and (ii) two-way coupling simulations of decaying HIT. The computational domain of both simulation types is a cube with periodic boundary conditions in all directions and an edge length of L. Time quantities are given with respect to a reference time $T_{\mathrm{ref}} = L/\sqrt{2/3\langle K\rangle}$, where $\langle K\rangle$ is the average kinetic energy of the fluid.

The setup of the single-phase flow simulations is summarized in Table I. The given values correspond to the statistically steady state of the flow (before the decay) without the particles. The two-way coupled simulations also undergo a two-way coupled forcing period to obtain a statistically steady state before the forcing is turned off. The symbols in the table correspond to the Taylor-Reynolds number Re_λ, the turbulent Reynolds number based on the integral length scale Re_l, the Kolmogorov timescale τ_η, the Taylor microscale λ, and the longitudinal integral length scale l_{11}.

The DNS are carried out on a grid consisting of $N^3 = 256^3$ grid cells, which leads to a product of the maximum resolvable wave number k_{max} and the Kolmogorov length scale of $k_{\mathrm{max}}\eta = 1.37$. The LES are solved on a grid with $N^3 = 32^3$ cells.

2. Particle setups of the one-way coupled case

In the one-way coupled case, particles of five different Stokes numbers, $\mathrm{St} = \tau_p/\tau_\eta$, are introduced in the previously defined flow setup. The Stokes numbers are based on the Kolmogorov timescale of the statistically steady single phase flow. Since in the one-way coupling simulations the flow does not experience any feedback by the particles, the previously defined parameters of the flow do not change.

The particle relaxation time, $\tau_p = \rho_p d_p^2/(18\rho_{\mathrm{f}}\nu_{\mathrm{f}})$, the number of particles of the respective simulation N_{p}, and the particle diameter to mesh spacing ratio $d_p/\Delta h$ are summarized in Table II. In

TABLE II. Particle configurations of the one-way coupling case.

Parameter	St = 0.5	St = 1	St = 2	St = 4	St = 8
τ_p/T_{ref}	0.0037	0.0075	0.015	0.03	0.06
N_{p}	480115	480115	480115	480115	480115
$d_p/\Delta h$	0.2	0.2	0.2	0.2	0.2

TABLE III. Particle configurations of the two-way coupling case.

Parameter	St = 1	St = 2	St = 8
τ_p/T_{ref}	0.0075	0.015	0.060
N_{p}	91377408	45830011	12057066
$d_p/\Delta h$	0.1	0.1	0.1
ϕ	1.0	1.0	1.0

the one-way coupled simulation cases, the ratio of the particle diameter to the Kolmogorov length scale is $d_p/\eta = 0.047$ for all Stokes numbers.

The simulations run more than $150\tau_\eta$ before the statistics are evaluated to obtain converged statistics that are independent of the initial conditions.

3. Particle setups of the two-way coupled case

Two simulation configurations are performed, including two-way coupled particles of two different Stokes numbers. Both configurations are started with a period of forced turbulence until the particle-laden turbulence reaches a statistically steady state (at least $150\tau_\eta$). The decay of the turbulence and the tracking of the statistics starts after this forcing period. Note that the Kolmogorov timescale and thus also the Stokes numbers are based on the statistically steady single phase flow turbulence. In the one-way coupled simulation cases, the ratio of the particle diameter to the Kolmogorov length scale is $d_p/\eta = 0.023$, and the particle mass fraction is $\phi = 1.0$, for all Stokes numbers. The particle related parameters of the two two-way coupled simulations are summarized in Table III.

4. Parameters of the modeling framework

Besides the DNS and the classical LES, we also conduct simulations using the proposed LES modeling framework. For the mLDKM part of the modeling framework, there are no tunable model parameters that have to be specified. The model for the subgrid-scale velocity however, requires us to choose some parameters. It was shown by Hausmann *et al.* [32] that the statistics of the subgrid-scale velocity are relatively insensitive to the values of these parameters.

The number of statistically homogeneous subdomains, N_{domain}, depends on the characteristic length scales at which the statistics of the subgrid-scale velocity vary. Based on experience, we suggest choosing the size of a subdomain approximately four times the size of a LES grid cell per direction. Note that in previous studies, the number of subdomains did not critically influence the velocity statistics.

Another parameter is related to the interpolation between the subdomains to obtain a divergence-free velocity field. The interpolation kernel is [32]

$$W(r) = 1 - \frac{1}{1 + \mathrm{e}^{-\alpha r}}, \tag{36}$$

where r is the distance to the respective subdomain boundary, and α a parameter that determines the thickness of the region that is influenced by the interpolation. In general, the influence region of the interpolation should be as small as possible to keep the region that is not affected by the interpolation as large as possible. However, the influence region should not be so small that the particles experience the subdomain boundary as discontinuity of the subgrid-scale velocity. We empirically found that $\alpha = 40/\Delta h_{\text{domain}}$ works well for the considered cases, where Δh_{domain} is the width of a subdomain. It is shown in Appendix A that the clustering of the particles is not significantly influenced even if the parameter α is varied over a wide range.

The remaining parameter that has to be set is the number of modes N_{m} in the series expansion Eq. (27). Similar to the number of subdomains, it has been shown previously that the influence of

TABLE IV. Parameters of the model for the subgrid-scale velocity.

Parameter	Value
N_{domain}	8
α	$40/\Delta h_{\text{domain}}$
N_{m}	108

N_{m} on the velocity statistics is negligible as long as $N_{\text{m}} = O(10^2)$. The particular choice for N_{m} in the present paper is mainly based on load balancing considerations. Although we did not observe the results to sensitively depend on the choice of the number of modes in our previous study [32], we cannot exclude that as the range of modeled scales increases significantly, e.g., by a significantly larger Re_λ, the number of modes needs to increase accordingly. The values of the parameters in the present paper are summarized in Table IV.

V. RESULTS AND DISCUSSIONS

A. One-way coupled configurations

In this section, the configurations described in Sec. IV B 2 are investigated. In the following, it is referred to as enriched LES if the particles are propagated with a drag force based on the sum of the LES velocity and the modeled subgrid-scale velocity at the particle positions.

The particle pair dispersion is evaluated in the enriched LES, the classical LES, and the DNS. The particle pair dispersion is defined as the ensemble-averaged and time-dependent distance between particle pairs, whereas a particle pair is considered as two particles with an initial separation of the Kolmogorov length scale,

$$\langle \delta \rangle(t) = \langle |\boldsymbol{x}_{p0}(t) - \boldsymbol{x}_{p1}(t)| \rangle, \tag{37}$$

where $\boldsymbol{x}_{p0}(t)$ and $\boldsymbol{x}_{p1}(t)$ are the positions of the particles belonging to a particle pair and $\langle \delta \rangle(t = 0) = \eta$.

The particle pair dispersion in the DNS, the classical LES, and the enriched LES for the five different Stokes numbers of the one-way coupling case is depicted in Fig. 2. It can be observed that for all the considered Stokes numbers, the particle pairs stay together for a short time before they disperse rapidly. Eventually, the average separation reaches a steady state, which corresponds approximately to the half domain size, indicating that the maximum separation that is possible in a fully periodic cubic domain is reached. For higher Stokes numbers, the particle pairs stay close to each other for a shorter time, as particles with a large Stokes numbers are more likely to have different velocities caused by their high inertia. The classical LES predicts the particle pairs to disperse much slower than in the DNS due to the missing effect of the subgrid-scale velocity sweeping the particles into regions of different large scale velocities. This effect is observed for all investigated Stokes numbers, but is slightly more dominant for the larger Stokes numbers.

In the enriched LES, the predicted particle pair dispersion almost overlaps with those of the DNS. An important reason why the enriched LES performs so well is that the subgrid-scale velocity at the particle position is computed from a spatially continuous velocity field. As a consequence, two particles that are very close also experience a similar subgrid-scale velocity. This is not the case for Lagrangian models (see, e.g., Fede *et al.* [5], Bini and Jones [6], Pozorski and Apte [9]), which typically solve an evolution equation for each particle individually. Lagrangian models typically perform poorly in particle pair dispersion [53].

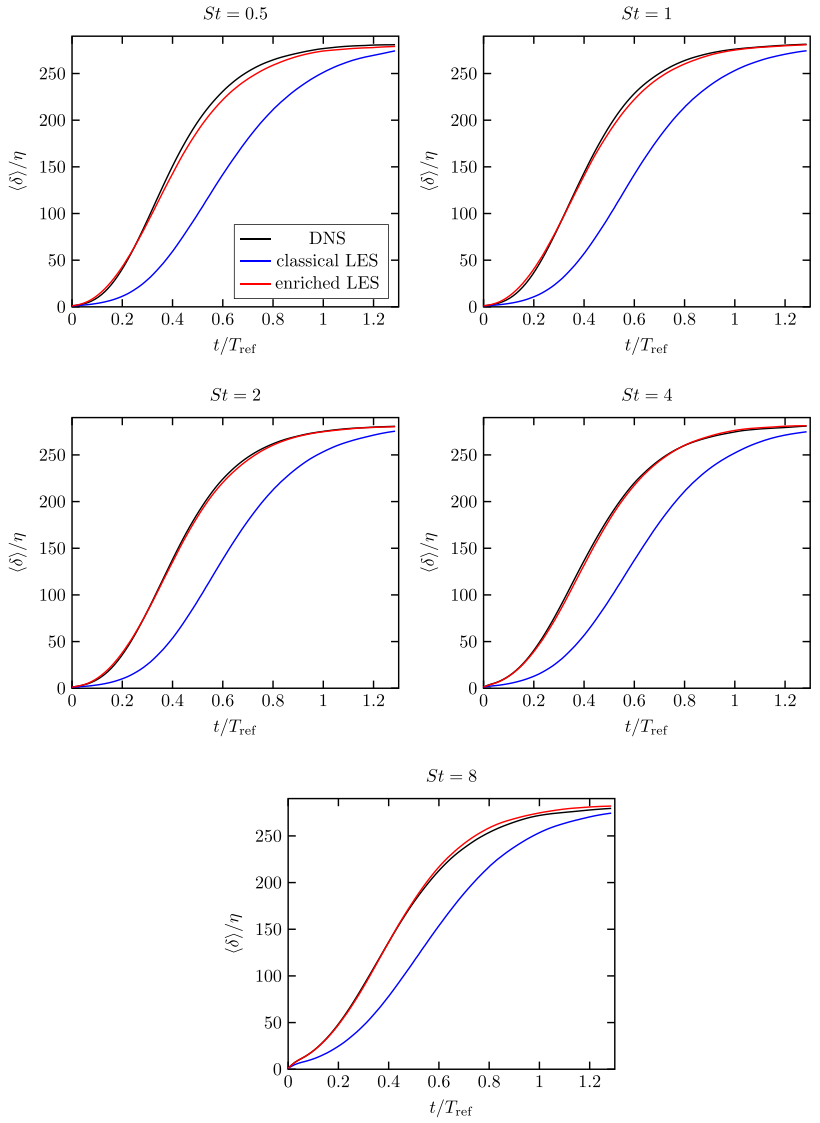

FIG. 2. Particle pair dispersion of the one-way coupled simulations for different Stokes numbers in forced HIT with the flow parameters given in Table I. The results are shown for the DNS, the classical LES, and the enriched LES.

A property that is of high practical importance is the extent with which particles form clusters. Particle clustering can be quantified by the radial distribution function, defined as

$$g(r) = \left\langle \frac{N_{\mathrm{p},i}(r)/\Delta V_i(r)}{N_\mathrm{p}/V} \right\rangle, \tag{38}$$

where $N_{\mathrm{p},i}(r)$ is the number of particles in a spherical shell with radius r centered at the location of the original particle and $V_i(r)$ is the volume of this spherical shell. The radial distribution function is normalized by the total number of particles N_p and the total volume of the domain V. Values of $g > 1$ indicate particle clustering and $g = 1$ uniformly distributed particles.

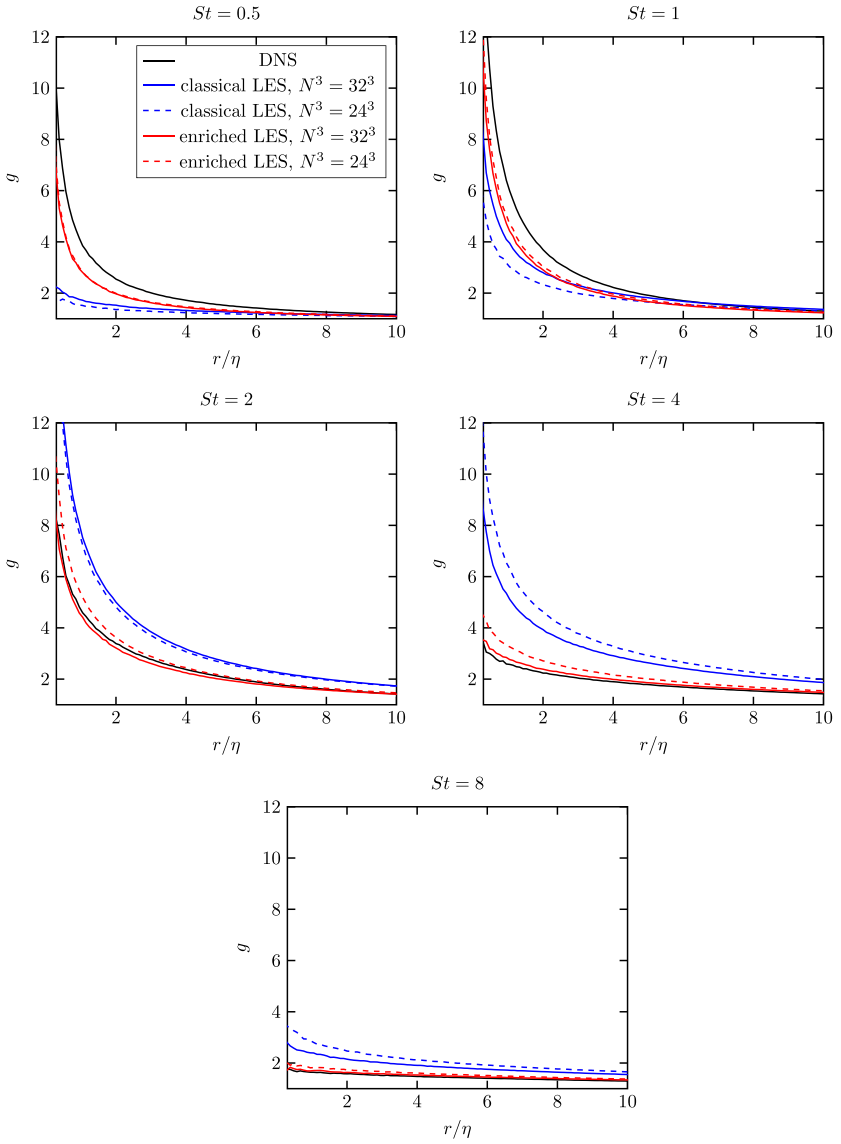

FIG. 3. Radial distribution function of the one-way coupled simulations for different Stokes numbers in forced HIT with the flow parameters given in Table I. The results are shown for the DNS, the classical LES, and the enriched LES. The results of the classical LES and the enriched LES are additionally shown with a coarser resolution of $N^3 = 24^3$ cells.

In Fig. 3, the radial distribution functions are shown. In addition to the LES simulations using $N^3 = 32^3$ cells, we also investigate particle clustering as a key statistic for assessing the influence of turbulence on particles in an even coarser LES, using $N^3 = 24^3$ cells. The setup for the enriched LES is similar to that of the LES with $N^3 = 32^3$ cells, with the exception of the number of subdomains. According to the presented guidelines, $N^3 = 24^3$ cells require $N_{\text{domain}} = 6$ subdomains, with each subdomain size corresponding to four times the size of a LES cell per direction. We have shown that other parameters have little influence on the observed fluid statistics [32].

The clustering reaches its maximum at $\mathrm{St} \approx 1$. For smaller and larger Stokes numbers, clustering is reduced. The classical LES yields an underestimation of the clustering for $\mathrm{St} = 0.5$ and $\mathrm{St} = 1$ and to an overestimation of the clustering for the Stokes numbers $\mathrm{St} = 2$, $\mathrm{St} = 4$, and $\mathrm{St} = 8$. This phenomenon has also been observed in previous studies [2,14,17]. This means that the modeled subgrid-scale velocity has to increase the clustering for the small St and increase the dispersion for the larger St. Note that increasing the particle dispersion is much simpler to achieve than increasing the particle clustering. In fact, the relations between strain and rotation of the velocity field are crucial for the correct prediction of particle clustering [54,55].

The enriched LES using $N^3 = 32^3$ cells shows that for Stokes numbers $\mathrm{St} = 2$, $\mathrm{St} = 4$, and $\mathrm{St} = 8$, particle clustering almost matches the clustering predicted by the DNS. When using a coarser resolution, clustering slightly increases, and the radial distribution function obtained from the enriched LES shows a small deviation from the DNS radial distribution function. For the Stokes numbers $\mathrm{St} = 4$ and $\mathrm{St} = 8$, a similar increase in clustering is observed in classical LES using $N^3 = 24^3$ cells. Therefore, the more accurate prediction of clustering behavior observed in the enriched LES is relatively independent of the LES resolution for these Stokes numbers.

For Stokes numbers $\mathrm{St} = 0.5$ and $\mathrm{St} = 1$, particle clustering is increased by the enriched LES compared to classical LES. However, the agreement with the DNS is not as good as for higher Stokes numbers, and the improvement in the radial distribution function for $\mathrm{St} = 1$ is minor. With a coarser grid of $N^3 = 24^3$ cells, the radial distribution function of the enriched LES remains almost unchanged, while the clustering intensity of the classical LES is further reduced due to the coarser resolution.

Our previous study [32] has shown that the probability distribution function (PDF) of the second invariant of the velocity gradient tensor is significantly improved with the enriched LES compared to the classical LES, which explains the ability of the model to increase the clustering of particles with small Stokes numbers.

The kinetic energy of the classical LES relative to the kinetic energy of the DNS is $K_{\mathrm{LES}}/K_{\mathrm{DNS}} \approx 0.83$. Together with the estimated subgrid-scale kinetic energy, this gives $(K_{\mathrm{LES}} + K_{\mathrm{sgs}})/K_{\mathrm{DNS}} \approx 1.07$. The fact that the total kinetic energy of the enriched LES overpredicts the kinetic energy of the DNS is important for the interpretation of the following results.

Figure 4 shows the PDF of the cosine of the angles between the particle velocity and the fluid velocity at the particle position, together with the mean values. The most likely event for all the considered Stokes numbers is the case where the fluid velocity is aligned with the particle velocity. However, for increasing Stokes numbers the probability of larger angles between the fluid velocity and the particle velocity also increases. Except for $\mathrm{St} = 0.5$, the classical LES always predicts too strong an alignment of fluid and particle velocities. For higher Stokes numbers, in particular, the particles are too heavy to follow the subgrid-scale velocity fluctuations, which typically change with high frequency and small magnitude. In the classical LES, these fluctuations are missing. The enriched LES provides the subgrid-scale fluctuations, which explains the improved PDF and means of velocity alignment for larger Stokes numbers. However, for Stokes numbers $\mathrm{St} = 0.5$, $\mathrm{St} = 1$, and $\mathrm{St} = 2$, the enriched LES does not improve the results of the classical LES. It is worth noting, however, that when considering all Stokes numbers, the prediction of the mean angle between the fluid velocity and the particle velocity is better for the enriched LES, as the absolute deviations from the mean angle of the DNS increase with the Stokes number. One possible reason for the deviation for $\mathrm{St} = 0.5$ and $\mathrm{St} = 1$ is that it is caused by the too-high kinetic energy of the enriched LES. Therefore, the particles with the small Stokes numbers cannot follow the velocity fluctuations as well as in the case of the DNS and the classical LES. For higher Stokes numbers, the deviation between the velocities is more significant and the higher subgrid-scale kinetic energy has a smaller influence.

From the results of the one-way coupled simulations, it can be concluded that the enrichment with subgrid-scale velocity can significantly improve the particle statistics in HIT for Stokes numbers $\mathrm{St} \geqslant 2$. Particularly worth highlighting is that the clustering can be improved for both qualitatively different cases of $\mathrm{St} \leqslant 1$ and $\mathrm{St} > 1$ with the modeled subgrid-scale velocity although the improvements for the smaller Stokes numbers are less pronounced.

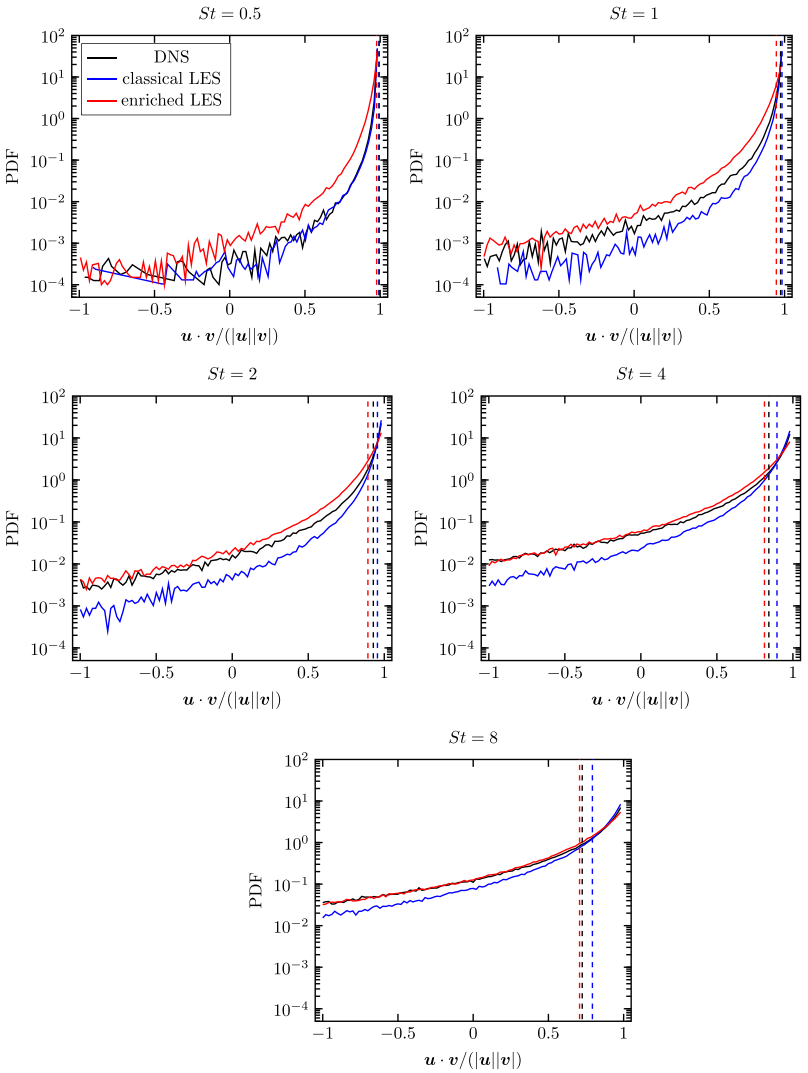

FIG. 4. PDF of cosine of angle between the fluid velocity at the particle position and the particle velocity of the one-way coupled simulations for different Stokes numbers in forced HIT with the flow parameters given in Table I. The results are shown for the DNS, the classical LES, and the enriched LES. The vertical lines indicate the respective mean value.

The computational cost of the proposed model is of high practical relevance, but it strongly depends on the specific configuration being considered. Solving for the enriched LES velocity approximately doubles the computational cost compared to the classical LES. However, there is an additional computational cost if particles are transported, namely, the subgrid-scale velocity interpolation to each particle position. For example, in the present one-way coupled simulations, the enriched LES with 2.4 million particles is six to seven times more expensive than the classical LES without enrichment. However, the total enriched framework is still orders of magnitude cheaper than the DNS.

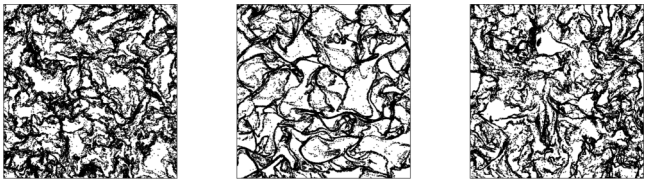

(a) (b) (c)

FIG. 5. Particle positions of the two-way coupled simulations with St = 2 of HIT with the flow parameters given in Table I. The results are evaluated at the last forced time step. The particle positions are projected from a slice of thickness equal to the Kolmogorov length scale η. (a) shows the particles of the DNS, (b) the particles of the classical LES, and (c) the particles of the modeled LES.

B. Two-way coupled configurations

In the present section, the modification of the turbulent flow by the particles is considered, which enables the assessment of the full modeling framework including the modeling of the subgrid-scale velocity combined with the mLDKM (previously introduced as modeled LES).

In Fig. 5, the projected particles in a slice of the thickness η are plotted for the case of St = 2 for the DNS, the classical LES, and the modeled LES. The positions are evaluated at the end of the forcing period. The particles reached steady statistics at this point in time.

The shapes of the clusters that are formed by the DNS and the classical LES differ significantly. The clusters of the classical LES are much coarser and more pronounced than the clusters of the DNS. The additional subgrid-scale velocity of the modeled LES breaks up the large clusters of the classical LES into clusters of smaller size, which are also less dense.

Figure 6 shows the kinetic energy spectra of the two-way coupled simulations for St = 1, St = 2, and St = 8, respectively. Due to the interaction with the particles, the results obtained with the DNS deviate significantly from the inertial range slope of single phase turbulence. In addition to the DNS, the results of the classical LES and the modeled LES are depicted. The kinetic energy spectrum that is resolved by the LES grid is shown separately from the kinetic energy spectrum of the modeled subgrid-scale velocity.

The filter imposed by the spatially varying turbulent viscosity is unknown. To achieve realistic particle transport, it is advantageous if the kinetic energy spectrum of the LES is similar to that of the DNS. In other words, it is desirable that the turbulent viscosity imposes a filter that closely resembles a spectrally sharp filter.

The classical LES overestimates the subgrid-scale fluid dissipation, resulting in a deviation from the slope of the DNS spectrum. The modeled LES takes into account the reduced subgrid-scale fluid dissipation caused by particle dissipation. As a result, the modeled LES leads to a spectrum that is in better agreement with the DNS spectrum for all three Stokes numbers.

The kinetic energy spectrum of the modeled subgrid-scale velocity is in good agreement with the DNS spectrum but its shape deviates in all three cases. The shape of the modeled subgrid-scale kinetic energy spectrum is very similar for St = 1, St = 2, and St = 8 even though the shapes of the two DNS spectra are very different. The model for the subgrid-scale velocity does not receive any information on the presence of the particle, except for the kinetic energy. Therefore, the modeled subgrid-scale kinetic energy spectrum is a shifted spectrum that matches very well with a single phase flow spectrum [32].

A classical LES does not fully consider the interphase kinetic energy transfer, since the interactions of the subgrid-scale velocity with the particles and the unresolved particle motion with the resolved flow scales are neglected. For small-particle Reynolds numbers, the kinetic energy transfer is proportional to the fluid velocity times the Stokes drag, $\boldsymbol{u} \cdot (\boldsymbol{v} - \boldsymbol{u})/\tau_p$, which is plotted in Fig. 7 for the present cases. Negative values indicate that kinetic energy is removed from the fluid and positive values correspond to kinetic energy that is added to the fluid by the particles. Note that, as

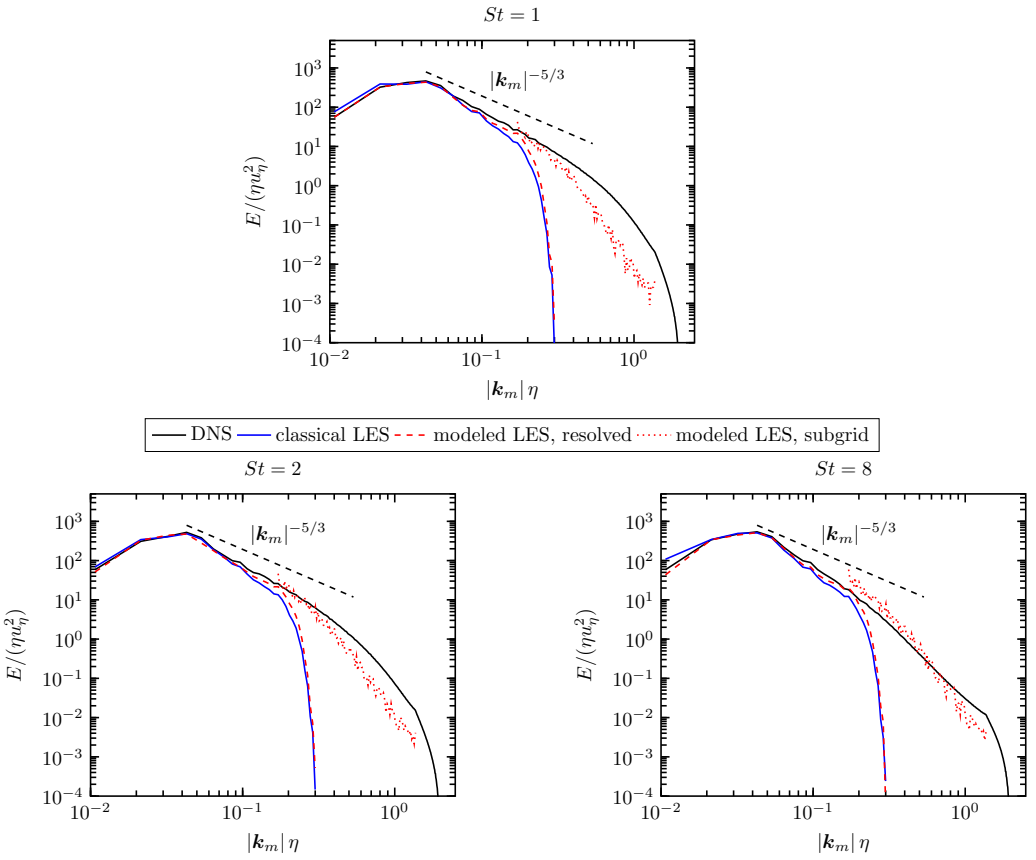

FIG. 6. Kinetic energy spectrum of the two-way coupled simulations with St = 1, St = 2, and St = 8 of HIT with the flow parameters given in Table I. The results are evaluated at the last forced time step. Compared are the DNS, the classical LES, and the modeled LES. The spectrum of the modeled LES is split into a part that is resolved by the LES grid and a subgrid-scale contribution that is modeled.

shown by Xu and Subramaniam [56], the energy that is removed from the fluid does not necessarily equal the kinetic energy that is added to the particles in a point-particle simulation.

The PDF in Fig. 7 shows a negative mean value for all Stokes numbers, indicating that, on average, the particles remove energy from the fluid. The PDF becomes wider and possesses larger absolute mean values as the Stokes number increases. The classical LES underpredicts the absolute of the mean values of the DNS for all Stokes numbers. With the proposed modeled LES, the kinetic energy that is removed by the particles is increased, which is qualitatively similar to the behavior of the DNS relative to the classical LES. In the classical LES, the particle velocities tend to align more with the local fluid velocity compared to the DNS because of the absence of small vortices that the particles cannot follow. With the proposed modeling, small velocity structures are provided, which increases the absolute energy transfer. However, for all Stokes numbers the width of the PDFs is overpredicted by the modeled LES.

The second effect that is neglected in a classical LES is the reduced subgrid-scale kinetic energy due to the turbulence modification by the particles. The subgrid-scale kinetic energies over time are depicted in Fig. 8. The subgrid-scale kinetic energy of the DNS is computed by subtracting the kinetic energy of the spectrally sharp filtered DNS from the kinetic energy of the DNS. Since the actual filter of a LES imposed by the turbulent viscosity is unknown, the DNS is also

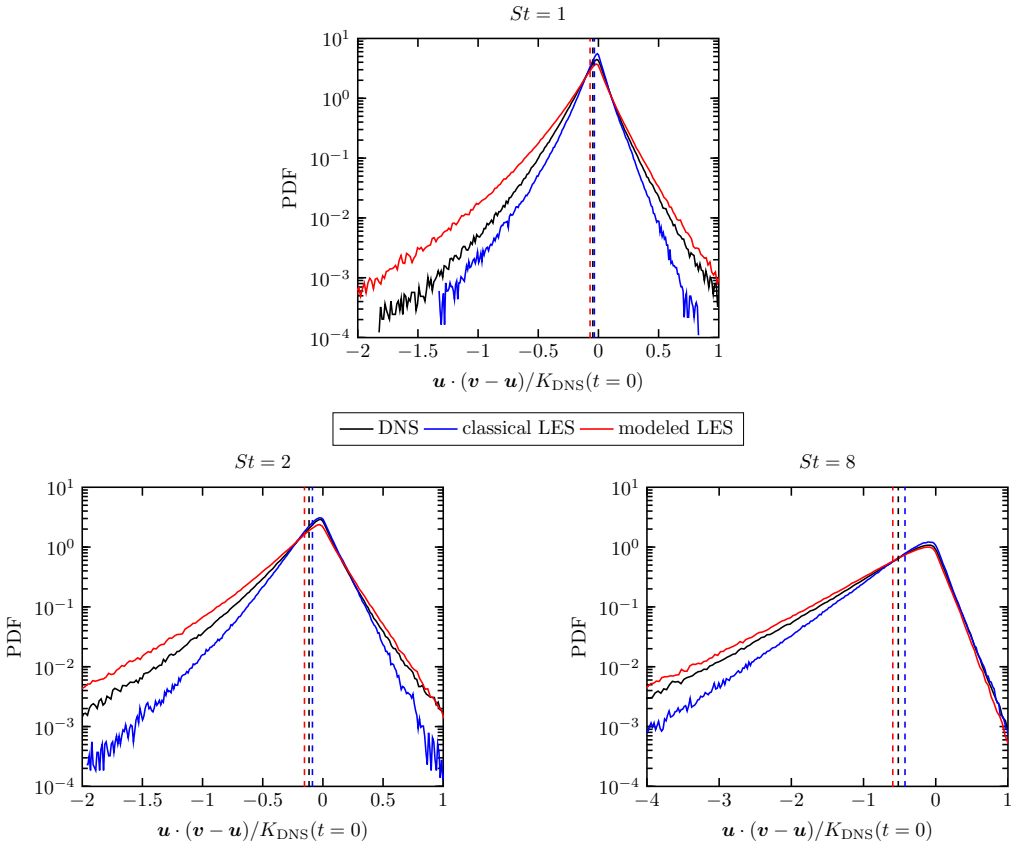

FIG. 7. PDF of the kinetic energy transfer between fluid and particles of the two-way coupled simulations with St = 1, St = 2, and St = 8 of HIT with the flow parameters given in Table I. The results are evaluated at the last forced time step. The vertical lines indicate the respective mean values.

volume averaged for comparison. The kinetic energies of the LES are obtained from the transport equation in the LDKM and mLKDM, respectively. It is observed that for all Stokes numbers, the classical LES predicts a much higher subgrid-scale kinetic energy than the DNS. The subgrid-scale kinetic energy of the modeled LES is significantly smaller because of the source term Φ_P in the transport equation for the subgrid-scale kinetic energy. A higher subgrid-scale kinetic energy yields a higher eddy viscosity and thus more subgrid-scale dissipation. The classical LES overpredicts the kinetic energy of the subgrid-scale velocity because the particle dissipation at high wave numbers is not accounted for. The additional source term in the subgrid-scale kinetic energy equation of the mLDKM considers the effect of the particles on the subgrid-scale quantities. The choice of the explicit filter introduces uncertainties that complicate the quantitative comparison of the LES predictions with the DNS. Nonetheless, the reduction of subgrid-scale kinetic energy is qualitatively consistent with the results obtained from explicitly filtering the DNS.

It is observed that the effects that are neglected in a classical LES act in opposite directions for the considered configurations. While the classical LES underpredicts the dissipation by the particles, it over-predicts the dissipation of the subgrid-scale velocity. Thus, these two errors at least partially compensate each other, which in total may lead to fair agreement with the total kinetic energy of the DNS. However, the proposed modeled LES considers each effect (i.e., the increased particle dissipation and the reduced fluid dissipation) separately and does not rely on compensation of errors.

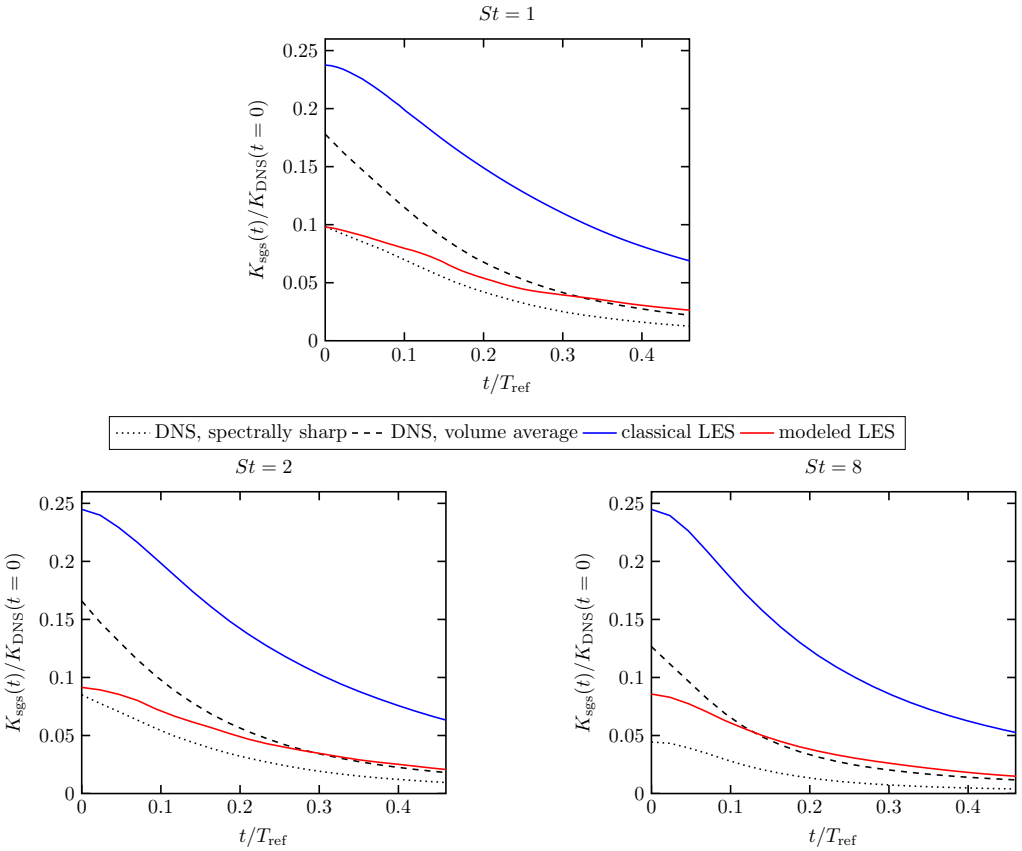

FIG. 8. Normalized subgrid-scale kinetic energy over time of the two-way coupled simulations with St = 1, St = 2, and St = 8 of decaying HIT with the flow parameters given in Table I. Compared are the results of the DNS (with a spectrally sharp filter and volume averaged), the classical LES, and the modeled LES with particle source term.

Figure 9 shows the normalized kinetic energy over time for the two-way coupled simulations with St = 1, St = 2, and St = 8, respectively. Besides the spectrally sharp filtered and volume averaged DNS (FDNS) and the classical LES, the results of the modeled LES are plotted. To investigate the influence of the particle source term Φ_P in the transport Eq. (18) of the subgrid-scale kinetic energy, the modeled LES is shown with the source term (modeled LES-mLDKM) and without the source term (modeled LES-LDKM). For St = 1 and St = 2, the LES, the modeled LES-mLDKM, and the modeled LES-LDKM predict a slower decay of the fluid kinetic energy than the DNS. The deviation of the three LES cases from the DNS is much smaller for St = 8. All Stokes numbers show only relatively small deviations between the LES cases. For St = 1, the kinetic energy predicted by the classical LES and the modeled LES-mLDKM are nearly identical. This is remarkable considering that the particle dissipation and fluid dissipation are significantly different between the two methods. The kinetic energy of the modeled LES-LDKM is always smaller than the kinetic energy of the modeled LES-mLDKM.

It is known from the literature that for Stokes numbers that are not significantly smaller than one, the total dissipation in a particle-laden flow is increased [19–21,23], which also applies to the Stokes numbers investigated in the present paper. The total dissipation has contributions from the particles and the fluid, as occurs in a single-phase flow. In a LES, the particle and the fluid dissipation have to

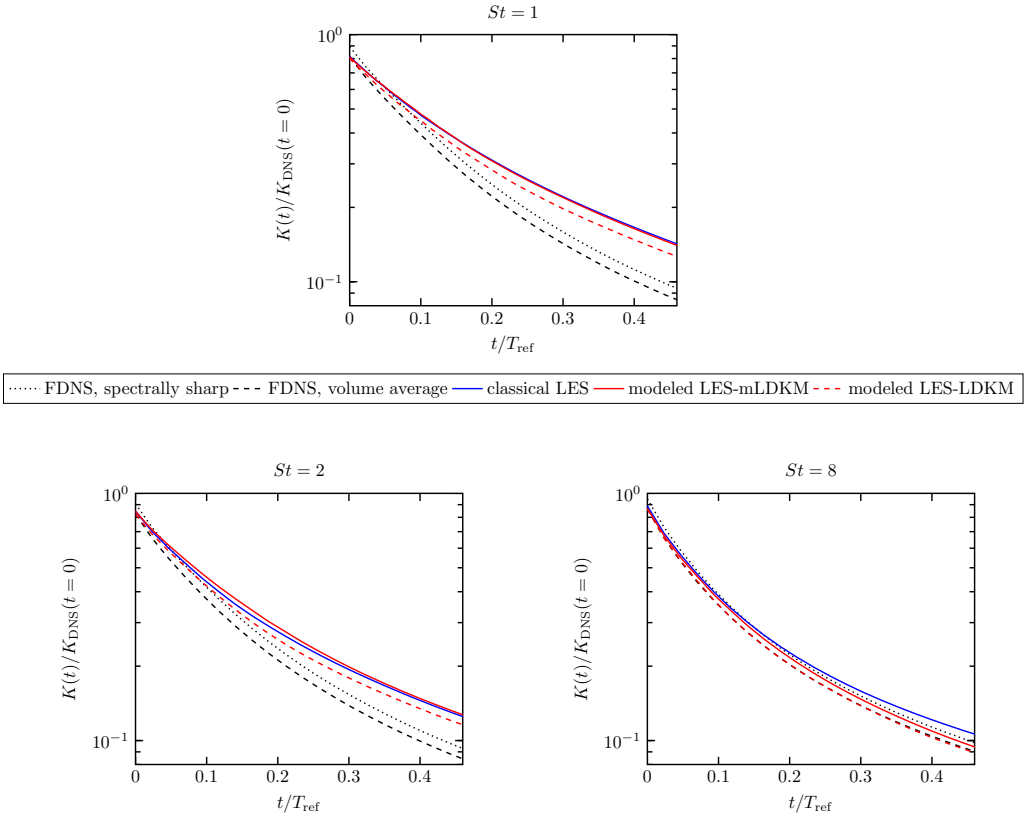

FIG. 9. Normalized kinetic energy over time of the two-way coupled simulations with St = 1, St = 2, and St = 8 of decaying HIT with the flow parameters given in Table I. Compared are the FDNS (with a spectrally sharp filter and volume averaged), the classical LES (LES-LDKM), the modeled LES with particle source term (modeled LES-mLDKM), and the modeled LES without particle source term (modeled LES-LDKM).

be modeled. As already pointed out, both contributions have opposite signs in the present cases. This becomes evident by the fact that the modeled LES without the particle source term Φ_P increases the total dissipation. The difference to the classical LES in this case is that the two-way coupling force is computed using the total fluid velocity consisting of the LES velocity and the modeled subgrid-scale velocity, which leads to increased dissipation relative to the classical LES. The dissipation by the particles yields a negative source term Φ_P, which reduces the subgrid-scale kinetic energy. This is why the total dissipation of the modeled LES-mLDKM is smaller than the total dissipation of the modeled LES-LDKM.

Note that both effects, the increased dissipation due to the particles and the reduced fluid dissipation, are at least qualitatively in agreement with the literature and desired. Since both effects act in opposite directions, the classical LES is still in acceptable agreement with the DNS even though it accounts for neither of the two effects.

We investigate the effect of LES resolution on two-way coupling statistics by conducting a coarser LES with $N^3 = 24^3$ cells of the two-way coupled simulation configuration with particles with a Stokes number St = 2. Figure 10 displays the results, which exhibit similar overall trends to those observed in the LES with $N^3 = 32^3$ cells. Notably, the shape of the kinetic energy spectrum of the modeled LES in Fig. 10(a) is closer to the DNS spectrum than the classical LES spectrum.

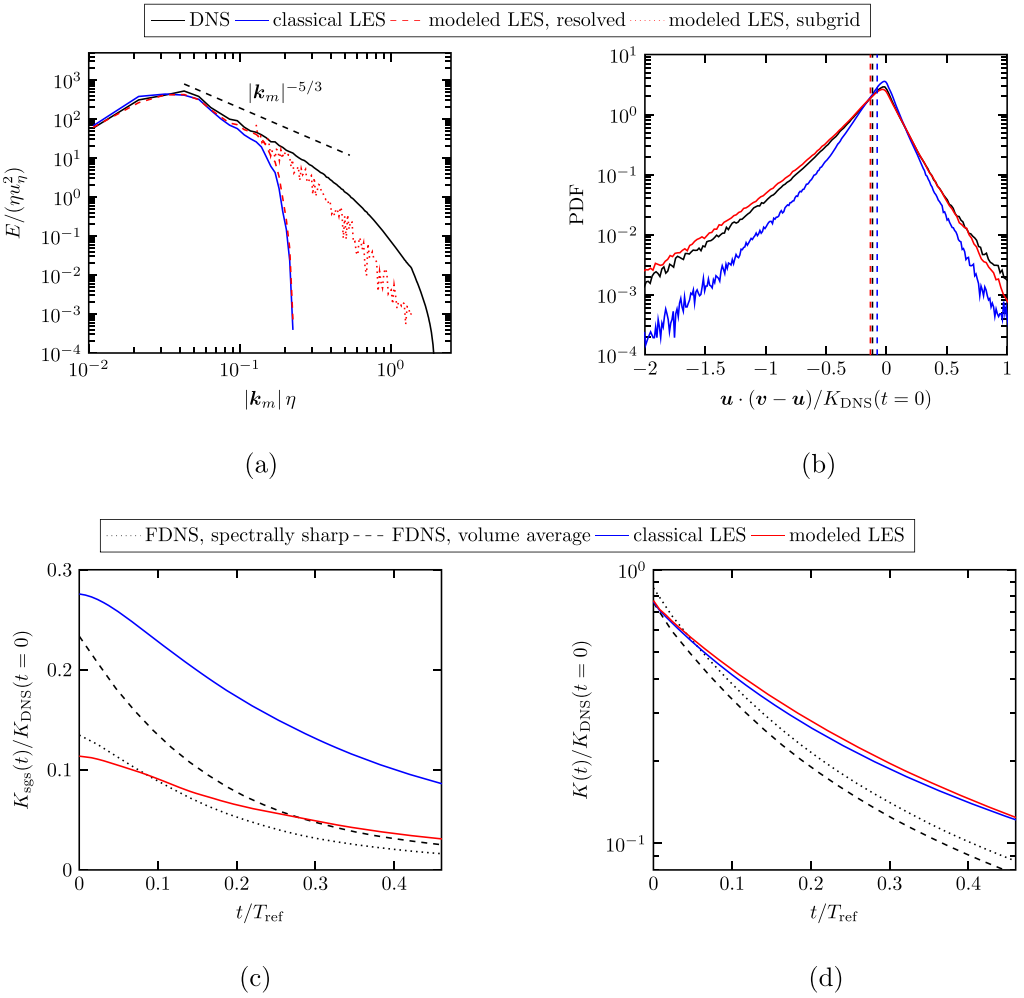

FIG. 10. Kinetic energy spectrum (a), PDF of the kinetic energy transfer between fluid and particles (b), subgrid-scale kinetic energy over time (c), and resolved kinetic energy over time (d) of decaying HIT with particles of Stokes number $\mathrm{St} = 2$ and the flow parameters given in Table I. Compared are the results of the DNS (with a spectrally sharp filter and volume averaged), the classical LES and the modeled LES with particle source term. The LES are performed on a grid of $N^3 = 24^3$ cells.

However, the subgrid-scale kinetic energy spectrum from the modeled LES underpredicts the DNS spectrum. In Fig. 10(b), it is noticeable that the classical LES predicts a PDF of the kinetic energy transfer that is too narrow, and this discrepancy is even more pronounced than in the higher resolution case. The modeled LES yields an improved shape of the PDF and the mean when compared to the classical LES. The subgrid-scale kinetic energy of the modeled LES is smaller, which leads to better agreement with the DNS results than the modeled LES with $N^3 = 24^3$ cells. The subgrid-scale kinetic energy is shown in Fig. 10(c). As expected, the predicted subgrid-scale kinetic energies are higher than with the finer resolution. The modeled LES reduces the too high subgrid-scale kinetic energy of the classical LES but predicts too small values during the beginning of the decay. The trends of the resolved kinetic energy in Fig. 10(d) are similar to the higher resolution. Both classical LES and modeled LES predict a too-slow decay of kinetic energy. The

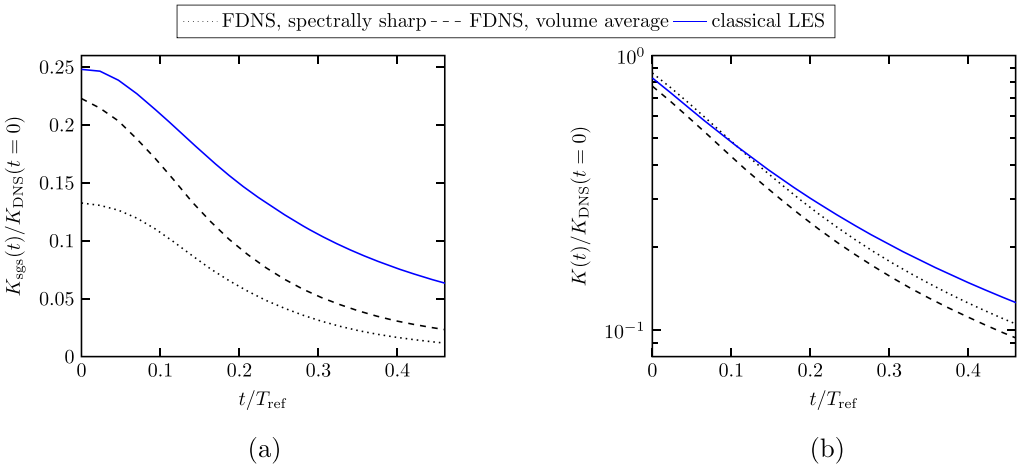

FIG. 11. Subgrid-scale kinetic energy over time (a) and resolved kinetic energy (b) of decaying HIT without particles and the flow parameters given in Table I. Compared are the results of the DNS (with a spectrally sharp filter and volume averaged) and the classical LES.

results of LES with $N^3 = 24^3$ cells suggest that the conclusions drawn for the proposed modeling framework qualitatively also apply to coarser LES.

To determine the source of the deviation of the resolved kinetic energy of the LES from the FDNS, it is instructive to investigate decaying single phase flow turbulence of the DNS and the classical LES with the LKDM. In Fig. 11, the subgrid-scale kinetic energy and the resolved kinetic energy of the classical LES are compared with DNS values that are obtained by explicit filtering. Owing to the uncertainties of the choice of the explicit filter, the spectrally sharp filtered and volume averaged DNS are both plotted. The subgrid-scale kinetic energy predicted by the LES is larger than the both estimations from the FDNS. The resolved kinetic energy of the LES shows the same discrepancy from the FDNS as the LES of the two-way coupled simulation, namely, a too-slow decay. If the subgrid-scale kinetic energy is too large and the decay of kinetic energy is too slow, it may be inferred that the primary source of error causing the inaccuracies lies in the computation of the viscosity constant C_k. On average, this constant seems to be too small, which results in the deviations of the modeled LES from the filtered DNS. It can be concluded that the introduced particle source term in the transport equation for the subgrid-scale kinetic energy plays a minor role in these inaccuracies, since the reduction of the predicted subgrid-scale kinetic energy and the increased particle dissipation are qualitatively captured by the model. The dynamical computation of C_k leaves space for future improvements of the model.

VI. CONCLUSIONS

In the present paper, we propose a model for predicting the behavior of two-way coupled particle-laden flow in the framework of LES. The model accounts for the interactions that are not captured by a classical LES of a particle-laden flow, which are (i) the prediction of the particle motion due to the missing subgrid-scale fluid velocity, (ii) the effect of the particles on the resolved flow scales, and (iii) the effect of the particles on the subgrid scales.

The proposed modeling framework consists of two components, a modeled transport equation for the subgrid-scale kinetic energy that includes a source term which accounts for the modification of the subgrid-scale kinetic energy by the particles and a model for the subgrid-scale velocity, which is used to close the particle equations of motion and the source-term in the transport equation for the subgrid-scale kinetic energy. The two model components are further coupled by directly using

the resulting subgrid-scale kinetic energy of the transport equation as input for the model for the subgrid-scale velocity that thus also accounts for the turbulence modulation of the subgrid-scales by the particles.

One-way coupled simulations are performed that are used to assess the isolated effect of missing subgrid-scale velocity in the computation of the forces acting on the particles and its modeling using the enriched LES. The proposed model accurately predicts particle pair-dispersion over a wide range of Stokes numbers using the modeled subgrid-scale velocity. Additionally, for Stokes numbers $\mathrm{St} \geqslant 2$, the model accurately recovers the particle clustering observed in the corresponding DNS simulations. For the challenging case of a small Stokes number ($\mathrm{St} = 0.5$), the model significantly improves particle clustering, while the improvement is less pronounced for $\mathrm{St} = 1$. The improvements achieved in the enriched LES come with computational costs that are reasonable within the scope of a LES. Furthermore, two-way coupled simulations of decaying HIT are carried out that require modeling of the turbulence modulation by the particles. The coupled framework yields an increased particle dissipation compared to the classical LES by considering the modeled subgrid-scale velocity in the feedback force. The subgrid-scale fluid dissipation is decreased relative to the classical LES because the mLDKM predicts a subgrid-scale kinetic energy that considers the turbulence modulation by the particles. Both effects are in agreement with the observed physics in a DNS. As a consequence, we observe a kinetic energy spectrum with the proposed modeling that is in good agreement with the spectrum observed in the DNS. We demonstrate that the predictions of the model are only weakly affected by changes in resolution of the LES while keeping Re_λ constant. However, investigating the ability of the model to accurately predict particle-turbulence interactions as the ratio between grid spacing and the Kolmogorov length scale, Δ/η, significantly increases, is an area that requires further investigation in future studies.

Finally, it is important to mention that the proposed modeling strategy possesses the prerequisites for simulating inhomogeneous and anisotropic flows since the subgrid-scale enrichment is formulated on a grid of statistically homogeneous subdomains, which allows for spatially varying statistics. Considering this, the present modeling framework has the potential to improve the capabilities of LES of particle-laden turbulent flows for a wide range of applications.

ACKNOWLEDGMENTS

This research was funded by the Deutsche Forschungsgemeinschaft (DFG, German Research Foundation—Project-ID No. 457509672.

APPENDIX

Figure 12 shows the radial distribution function of the one-way coupled simulations for different Stokes numbers and varying parameter α in the interpolation of the modeled subgrid-scale velocity between the subdomains. The parameter α is reduced and increased by a factor of 2 relative to the value $\alpha = 40$ that is used in the present paper, respectively. It can be observed that even for this relatively wide parameter range the radial distribution functions almost coincide. The particle clustering is thus essentially independent of α for the considered range of values.

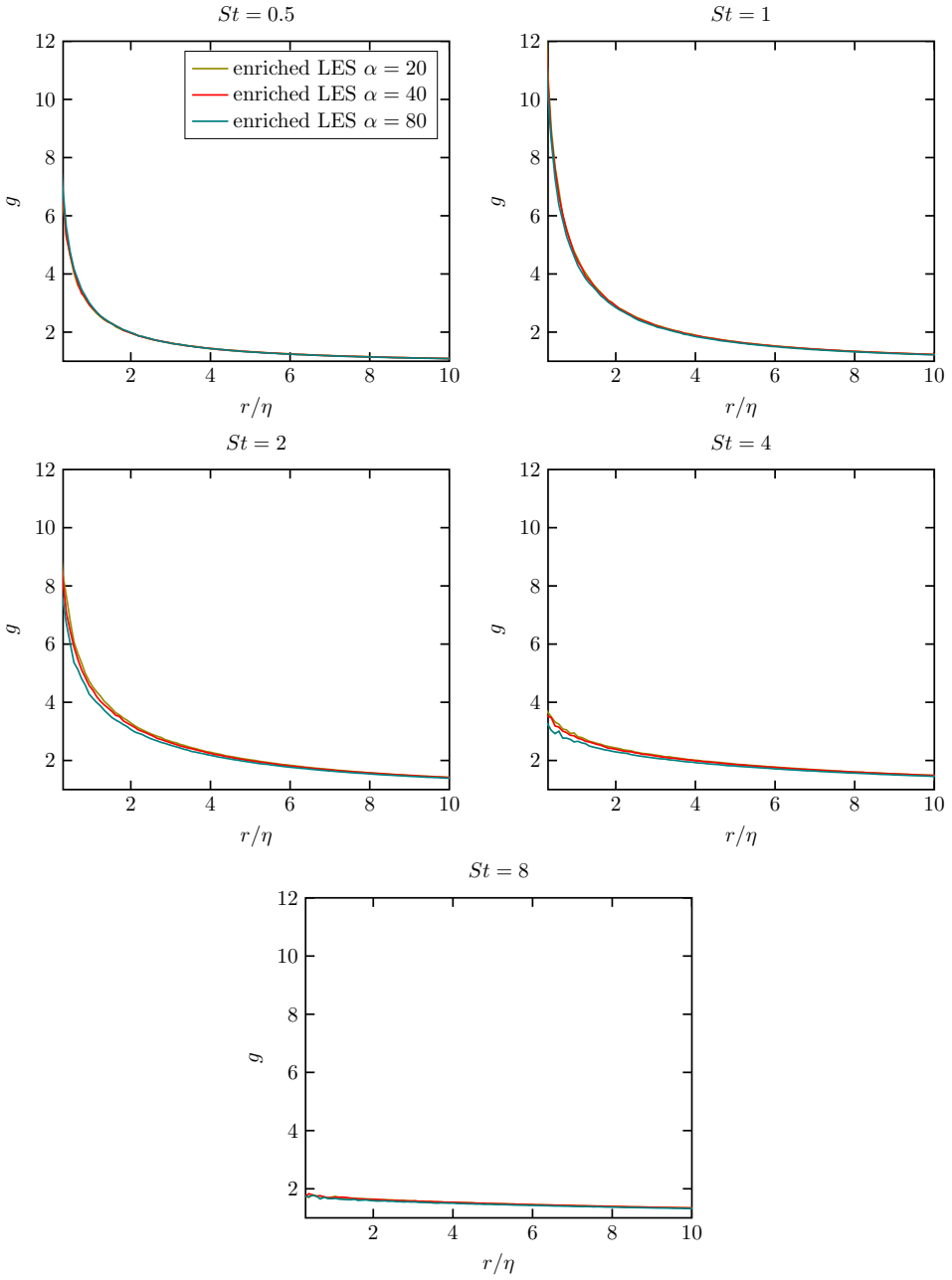

FIG. 12. Radial distribution function of the one-way coupling simulations for different Stokes numbers and different thickness constants α of the interpolation of the subgrid-scale velocity between the subdomains in forced HIT with the flow parameters given in Table I.

[1] V. Armenio, U. Piomelli, and V. Fiorotto, Effect of the subgrid scales on particle motion, Phys. Fluids **11**, 3030 (1999).

[2] B. Ray and L. R. Collins, Preferential concentration and relative velocity statistics of inertial particles in Navier–Stokes turbulence with and without filtering, J. Fluid Mech. **680**, 488 (2011).
[3] P. Fede and O. Simonin, Numerical study of the subgrid fluid turbulence effects on the statistics of heavy colliding particles, Phys. Fluids **18**, 045103 (2006).
[4] B. Rosa and J. Pozorski, Impact of subgrid fluid turbulence on inertial particles subject to gravity, J. Turbul. **18**, 634 (2017).
[5] P. Fede, O. Simonin, P. Villedieu, and K. D. Squires, Stochastic modeling of the turbulent subgrid fluid velocity along inertial particle trajectories, in *Proceedings of the Summer Program, Center for Turbulence Research, Stanford* (Citeseer, 2006), pp. 247–258.
[6] M. Bini and W. P. Jones, Particle acceleration in turbulent flows: A class of nonlinear stochastic models for intermittency, Phys. Fluids **19**, 035104 (2007).
[7] A. S. Berrouk, D. Laurence, J. J. Riley, and D. E. Stock, Stochastic modelling of inertial particle dispersion by subgrid motion for LES of high Reynolds number pipe flow, J. Turbul. **8**, N50 (2007).
[8] B. Shotorban and F. Mashayek, A stochastic model for particle motion in large-eddy simulation, J. Turbul. **7**, N18 (2006).
[9] J. Pozorski and S. Apte, Filtered particle tracking in isotropic turbulence and stochastic modeling of subgrid-scale dispersion, Int. J. Multiphase Flow **35**, 118 (2009).
[10] M. Knorps and J. Pozorski, Stochastic modeling for subgrid-scale particle dispersion in large-eddy simulation of inhomogeneous turbulence, Phys. Fluids **33**, 043323 (2021).
[11] J. G. M. Kuerten, Subgrid modeling in particle-laden channel flow, Phys. Fluids **18**, 025108 (2006).
[12] B. Shotorban and F. Mashayek, Modeling subgrid-scale effects on particles by approximate deconvolution, Phys. Fluids **17**, 081701 (2005).
[13] G. I. Park, M. Bassenne, J. Urzay, and P. Moin, A simple dynamic subgrid-scale model for LES of particle-laden turbulence, Phys. Rev. Fluids **2**, 044301 (2017).
[14] M. Bassenne, M. Esmaily, D. Livescu, P. Moin, and J. Urzay, A dynamic spectrally enriched subgrid-scale model for preferential concentration in particle-laden turbulence, Int. J. Multiphase Flow **116**, 270 (2019).
[15] J. A. Domaradzki and K.-C. Loh, The subgrid-scale estimation model in the physical space representation, Phys. Fluids **11**, 2330 (1999).
[16] B. Ray and L. R. Collins, A subgrid model for clustering of high-inertia particles in large-eddy simulations of turbulence, J. Turbul. **15**, 366 (2014).
[17] Z. Zhou, S. Wang, X. Yang, and G. Jin, A structural subgrid-scale model for the collision-related statistics of inertial particles in large-eddy simulations of isotropic turbulent flows, Phys. Fluids **32**, 095103 (2020).
[18] S. Murray, M. F. Lightstone, and S. Tullis, Single-particle Lagrangian and structure statistics in kinematically simulated particle-laden turbulent flows, Phys. Fluids **28**, 033302 (2016).
[19] G. Mallouppas, W. George, and B. van Wachem, Dissipation and inter-scale transfer in fully coupled particle and fluid motions in homogeneous isotropic forced turbulence, Int. J. Heat Fluid Flow **67**, 74 (2017).
[20] A. Ferrante and S. Elghobashi, On the physical mechanisms of two-way coupling in particle-laden isotropic turbulence, Phys. Fluids **15**, 315 (2003).
[21] R. Letournel, F. Laurent, M. Massot, and A. Vié, Modulation of homogeneous and isotropic turbulence by sub-Kolmogorov particles: Impact of particle field heterogeneity, Int. J. Multiphase Flow **125**, 103233 (2020).
[22] M. Boivin, O. Simonin, and K. D. Squires, Direct numerical simulation of turbulence modulation by particles in isotropic turbulence, J. Fluid Mech. **375**, 235 (1998).
[23] M. Nabavi, M. Di Renzo, and J. Kim, Modulation of interphase, cross-scale momentum transfer of turbulent flows by preferentially concentrated inertial particles, Phys. Rev. Fluids **7**, 044305 (2022).
[24] P. Sagaut, *Large Eddy Simulation for Incompressible Flows*, 3rd ed. (Springer, Berlin, 2005).
[25] M. Boivin, O. Simonin, and K. D. Squires, On the prediction of gas–solid flows with two-way coupling using large eddy simulation, Phys. Fluids **12**, 2080 (2000).
[26] N. Rohilla, P. Muramulla, and P. S. Goswami, Applicability of large eddy simulations to capture turbulence attenuation in particle-laden channel flows, Phys. Rev. Fluids **7**, 024302 (2022).

[27] S. Yuu, T. Ueno, and T. Umekage, Numerical simulation of the high Reynolds number slit nozzle gas-particle jet using subgrid-scale coupling large eddy simulation, Chem. Eng. Sci. **56**, 4293 (2001).
[28] S. Pannala and S. Menon, On LEM/LES methodology for two-phase flows, in *35th Joint Propulsion Conference and Exhibit* (American Institute of Aeronautics and Astronautics, Los Angeles, CA, 1999).
[29] V. Sankaran and S. Menon, LES of spray combustion in swirling flows, J. Turbul. **3**, N11 (2002).
[30] W.-W. Kim and S. Menon, An unsteady incompressible Navier-Stokes solver for large eddy simulation of turbulent flows, Int. J. Numer. Methods Fluids **31**, 983 (1999).
[31] S. Menon, P.-K. Yeung, and W.-W. Kim, Effect of subgrid models on the computed interscale energy transfer in isotropic turbulence, Computers & Fluids **25**, 165 (1996).
[32] M. Hausmann, F. Evrard, and B. van Wachem, An efficient model for subgrid-scale velocity enrichment for large-eddy simulations of turbulent flows, Phys. Fluids **34**, 115135 (2022).
[33] M. Maxey, Simulation methods for particulate flows and concentrated suspensions, Annu. Rev. Fluid Mech. **49**, 171 (2017).
[34] T. B. Anderson and R. Jackson, A fluid mechanical description of fluidized beds, I and EC Fundamentals **6**, 527 (1967).
[35] J. G. M. Kuerten, Point-particle DNS and LES of particle-laden turbulent flow—a state-of-the-art review, Flow, Turbul. Combust. **97**, 689 (2016).
[36] C. T. Crowe, M. P. Sharma, and D. E. Stock, The particle-source-in cell/PSI-CELL/model for gas-droplet flows, J. Fluids Eng. **99**, 325 (1977).
[37] U. Schumann, Subgrid scale model for finite difference simulations of turbulent flows in plane channels and annuli, J. Comput. Phys. **18**, 376 (1975).
[38] G. Mallouppas and B. van Wachem, Large eddy simulations of turbulent particle-laden channel flow, Int. J. Multiphase Flow **54**, 65 (2013).
[39] P. L. Johnson, On the role of vorticity stretching and strain self-amplification in the turbulence energy cascade, J. Fluid Mech. **922**, A3 (2021).
[40] D. K. Lilly, The representation of small scale turbulence in numerical simulation experiments, in *Proceedings of the IBM Scientific Computing Symposium on Environmental Sciences, Yorktown, NY, USA,* National Center for Atmospheric Research (USA), NCAR Manuscript No. 281 (1966), pp. 195–210.
[41] W.-W. Kim, S. Menon, W.-W. Kim, and S. Menon, Application of the localized dynamic subgrid-scale model to turbulent wall-bounded flows, in *35th Aerospace Sciences Meeting and Exhibit* (American Institute of Aeronautics and Astronautics, Reno, NV, 1997).
[42] M. Germano, U. Piomelli, P. Moin, and W. H. Cabot, A dynamic subgrid-scale eddy viscosity model, Phys. Fluids A **3**, 1760 (1991).
[43] J.-P. Laval, B. Dubrulle, and S. Nazarenko, Nonlocality and intermittency in three-dimensional turbulence, Phys. Fluids **13**, 1995 (2001).
[44] V. M. Canuto and M. S. Dubovikov, A dynamical model for turbulence. I. General formalism, Phys. Fluids **8**, 571 (1996).
[45] A. Yoshizawa, Statistical theory for compressible turbulent shear flows, with the application to subgrid modeling, Phys. Fluids **29**, 2152 (1986).
[46] P. Moin, K. Squires, W. Cabot, and S. Lee, A dynamic subgrid-scale model for compressible turbulence and scalar transport, Phys. Fluids **3**, 2746 (1991).
[47] F. Denner, F. Evrard, and B. van Wachem, Conservative finite-volume framework and pressure-based algorithm for flows of incompressible, ideal-gas and real-gas fluids at all speeds, J. Comput. Phys. **409**, 109348 (2020).
[48] P. Bartholomew, F. Denner, M. Abdol-Azis, A. Marquis, and B. van Wachem, Unified formulation of the momentum-weighted interpolation for collocated variable arrangements, J. Comput. Phys. **375**, 177 (2018).
[49] G. Mallouppas, W. K. George, and B. van Wachem, New forcing scheme to sustain particle-laden homogeneous and isotropic turbulence, Phys. Fluids **25**, 083304 (2013).
[50] L. Verlet, Computer "e" on classical fluids. I. Thermodynamical properties of Lennard-Jones molecules, Phys. Rev. **159**, 98 (1967).

[51] L. Schiller and A. Naumann, über die grundlegenden Berechnungen bei der Schwerkraftaufbereitung, Z. Ver. Dtsch. Ing. **77**, 318 (1933).
[52] G. Tóth and P. Roe, Divergence- and curl-preserving prolongation and restriction formulas, J. Comput. Phys. **180**, 736 (2002).
[53] C. Marchioli, Large-eddy simulation of turbulent dispersed flows: A review of modelling approaches, Acta Mech. **228**, 741 (2017).
[54] M. R. Maxey, The gravitational settling of aerosol particles in homogeneous turbulence and random flow fields, J. Fluid Mech. **174**, 441 (1987).
[55] L. Brandt and F. Coletti, Particle-laden turbulence: Progress and perspectives, Annu. Rev. Fluid Mech. **54**, 159 (2022).
[56] Y. Xu and S. Subramaniam, Consistent modeling of interphase turbulent kinetic energy transfer in particle-laden turbulent flows, Phys. Fluids **19**, 085101 (2007).